Lawrence Berkeley National Laboratory

Title
ANALYSIS OF V-PARTICLE DECAYS AT BEVATRON ENERGIES

Permalink
https://escholarship.org/uc/item/66w49688

Author
Armstrong, Baxter H.

Publication Date
1956-07-01

UNIVERSITY OF CALIFORNIA

Radiation Laboratory

BERKELEY, CALIFORNIA

DISCLAIMER

UNIVERSITY OF CALIFORNIA

Radiation Laboratory
Berkeley, California

ANALYSIS OF V-PARTICLE DECAYS AT BEVATRON ENERGIES

Baxter H. Armstrong

(Thesis)

July 1956

ANALYSIS OF V-PARTICLE DECAYS AT BEVATRON ENERGIES

Contents

ANALYSIS OF V-PARTICLE DECAYS AT BEVATRON ENERGIES

Baxter H. Armstrong

Radiation Laboratory
University of California
Berkeley, California

July 1956

ABSTRACT

Two hundred and twelve neutral V-particle decays are analyzed with respect to their angular and momentum distributions, Q values, and production ratios. These V particles were produced in the stainless steel walls of a 36-atmosphere hydrogen-filled diffusion cloud chamber, by π^--meson, neutron, and proton beams from the Berkeley Bevatron. Particular attention is paid to cloud-chamber bias effects. No correlation in the angle between production and decay planes is found for these decays, and it is shown that in some instances previous results showing small-angle preferences for this angle can be explained in terms of a cloud-chamber bias. There appears to be an excess of forward π^+ emission in the CMS of the θ^0 decays. Similarly there is an excess of backward-emitted protons for the Λ^0 decays, but this is at least partly due to bias. Some of the complicating effects of production in heavy nuclei are discussed in appendices, and an extensive collection of graphs useful for the dynamical analysis of neutral and charged V's is included. Four "anomalous" neutral V's were found among these decays that do not fit a Λ^0 or θ^0 decay mode.

ANALYSIS OF V-PARTICLE DECAYS AT BEVATRON ENERGIES

I. INTRODUCTION

Neutral and charged V particles, so called because of their characteristic V-shaped cloud-chamber tracks, were discovered in 1947 by Rochester and Butler,[1] who were making a study of cosmic-ray penetrating showers. Since then, the masses, lifetimes, and decay modes of certain of these new unstable particles have been rather well determined.[2] The spins are still unknown within the possibilities allowed by the decay modes, although these possibilities have been narrowed considerably for one of the V^0 particles, the Λ^0, by recent calculations by Karplus and Ruderman.[3] The original discovery was made in a cosmic-ray experiment, and most of the subsequent work has been done in experiments of this type, since the energy required to produce V particles is beyond the capability of any but the most recently developed accelerators.

Upon completion of accelerators in the billion-electron-volt region, it immediately became of interest to examine any V particles that might be produced by the accelerated particles of these high-energy machines. In addition to verifying the results of the cosmic-ray experiments under different experimental conditions, and improving the cumulative statistical accuracy of the defining parameters, it is possible to obtain information concerning the process producing these particles more readily in an accelerator experiment than in a cosmic-ray experiment. One customarily knows more about the energy or energy spectrum of the primary particle responsible for the production process in an accelerator experiment, as well as more about its identity. Upon successful operation of the Brookhaven Cosmotron, V particles were produced in its beams, and their characteristics have been reported.[4,5,6] The events described herein were obtained in experiments carried out by the University of California Cloud Chamber group with the Berkeley Bevatron since it became operative in 1954. Hence they are produced at, and have, higher energies than the Cosmotron V particles. These experiments at Berkeley consisted of exposing hydrogen in a 36-atmosphere diffusion cloud chamber[7] to the negative pi-meson beam, the neutron beam, and the scattered proton beams from the

Bevatron target. The 212 V's described in this thesis were obtained from a total of about 40,000 pictures taken during these experiments, and result from interactions in the wall of the cloud chamber.

This thesis is primarily concerned with the neutral V particles, which Thompson[2] defines by the decay modes:

$$\Lambda^0 \rightarrow p^+ + \pi^- + 37 \text{ Mev} ,$$

$$\theta^0 \rightarrow \pi^+ + \pi^- + 214 \text{ Mev} ,$$

with lifetimes of $3.7 \, ^{+0.6}_{-0.5} \times 10^{-10}$ and $1.7 \, ^{+0.6}_{-0.4} \times 10^{-10}$ second, respectively. Other types* were not obtained in these experiments in statistically significant numbers; however, the basic data of the few charged V particles obtained are included for completeness, with a few remarks on these particles.

The interest in these particles arises from the inability of present theory to explain their existence, their relative stability in view of their copious production, and their interactions with better-known particles. Some recent work by Gell-Mann and Pais[10] holds promise of explaining the stability in terms of a new quantum number and a classification of interactions, but the other factors remain in almost complete obscurity.

The dynamical equations convenient for analyzing neutral two-body particle decays have been thoroughly discussed in the literature.[13, 14, 15] For convenience, a résumé of these equations is given in Appendix A, along with graphs of the relation between the two visible momenta, and the opening or deflection angle (for neutral and charged V's respectively). These graphs were prepared by the University of California Radiation Laboratory Cloud Chamber Group to facilitate the identification of the various types of neutral and charged V decays, and it is hoped that their availability in this report will prove a convenience to other workers in this field.

---

*There is recent evidence[12] that alternate decay modes

$$\Lambda^0 \rightarrow n + \pi^0 , \quad \theta^0 \rightarrow \pi^0 + \pi^0$$

exist, but these modes are undetectable in this experiment.

II. EXPERIMENTAL PROCEDURE
AND REDUCTION OF OBSERVATIONS

Experimental Procedure and Measurements

The experimental arrangements[16, 17, 18, 19] and instruments[7, 20] employed to obtain photographs of V-particle decays, as well as the scanning,[20] reprojection,[20, 21] and measuring procedures, are those previously described. Figures 1A and B show the 36-atmosphere diffusion cloud chamber, Fig. 2 shows the "space table" used to make the track measurements, and Fig. 3 is a schematic drawing of the space table (actually an earlier and simpler version), showing how the measurements are made.

Figure 4 shows a V^0 decay event; the arrow at the top indicates the direction of the incident beam. The momentum of the beam particles was 4.5 ± 0.3 Bev/c for the negative pi-meson beam, 6.20 ± 0.05 Bev/c for the proton beam, and an unknown spectrum extending to 7:1 Bev/c for the neutron beam.

The sensitive region of the chamber was approximately 12 inches in diameter (slightly larger than the region enclosed by the fiducial crosses in Fig. 4) and about 2.25 inches high.

The pulsed magnet current was 4,000 amperes for the π^- and p^+ experiments, and 2,500 amperes for the neutron experiment. The resulting fields were nominally 21,400 and 15,300 gauss respectively, with maximum variations across the usable area of the chamber of about 10%.

Maps of the field as a function of position in the chamber to an accuracy of 1.5% are available for the two current values. The field magnitude used in determining the momentum of a track is the value at the center of the track. The maximum error to the expected from this procedure is 1.5% (with, however, a nominal value much less than this). For discussion of this error, see Appendix C.

Ionization estimates are those obtained by eye, and were not employed unless they were quite unambiguous.

The angular track variables measured are defined as follows (see Fig. 3):
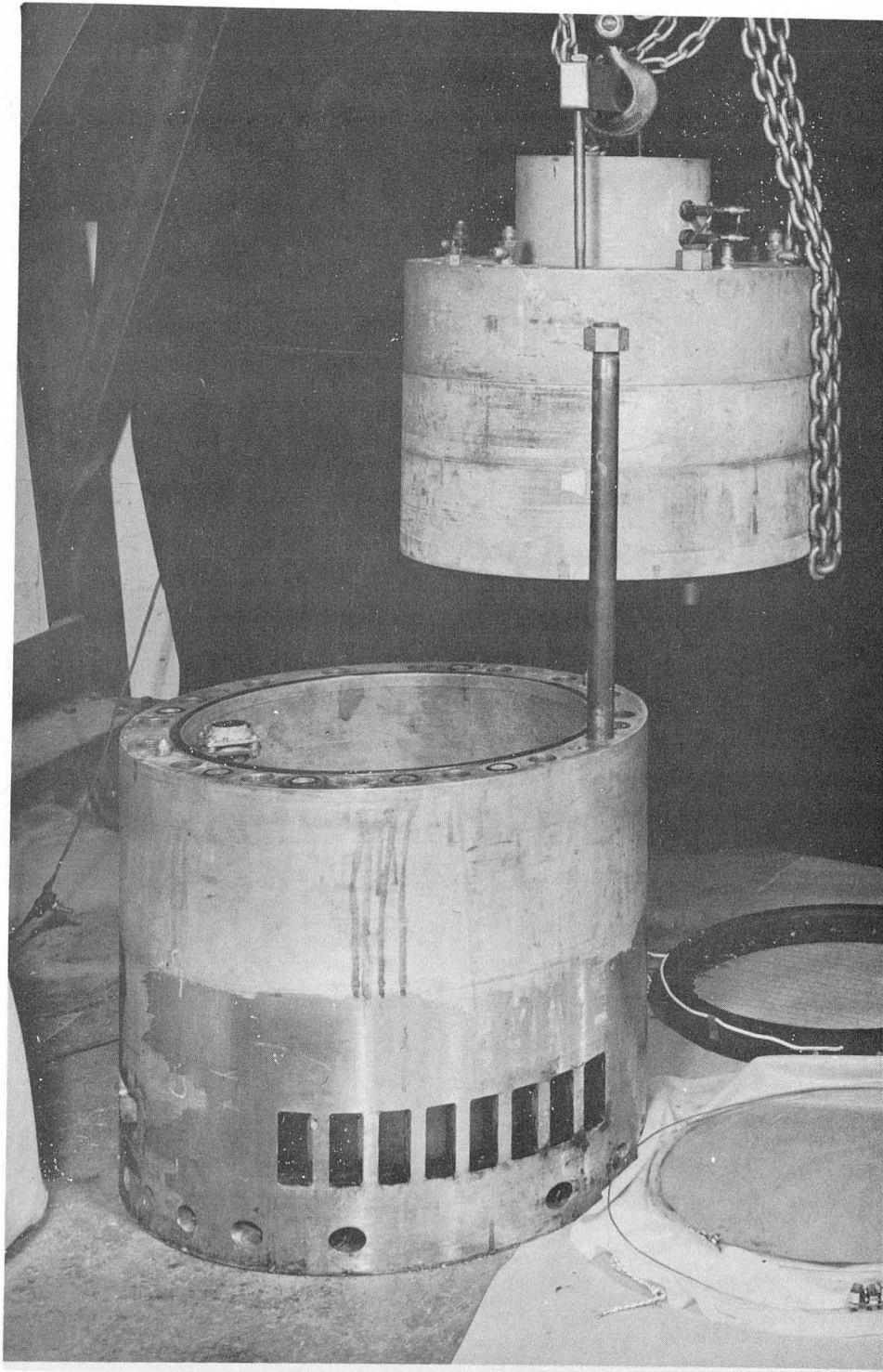
ZN-1175

Fig. 1A. The cloud chamber.
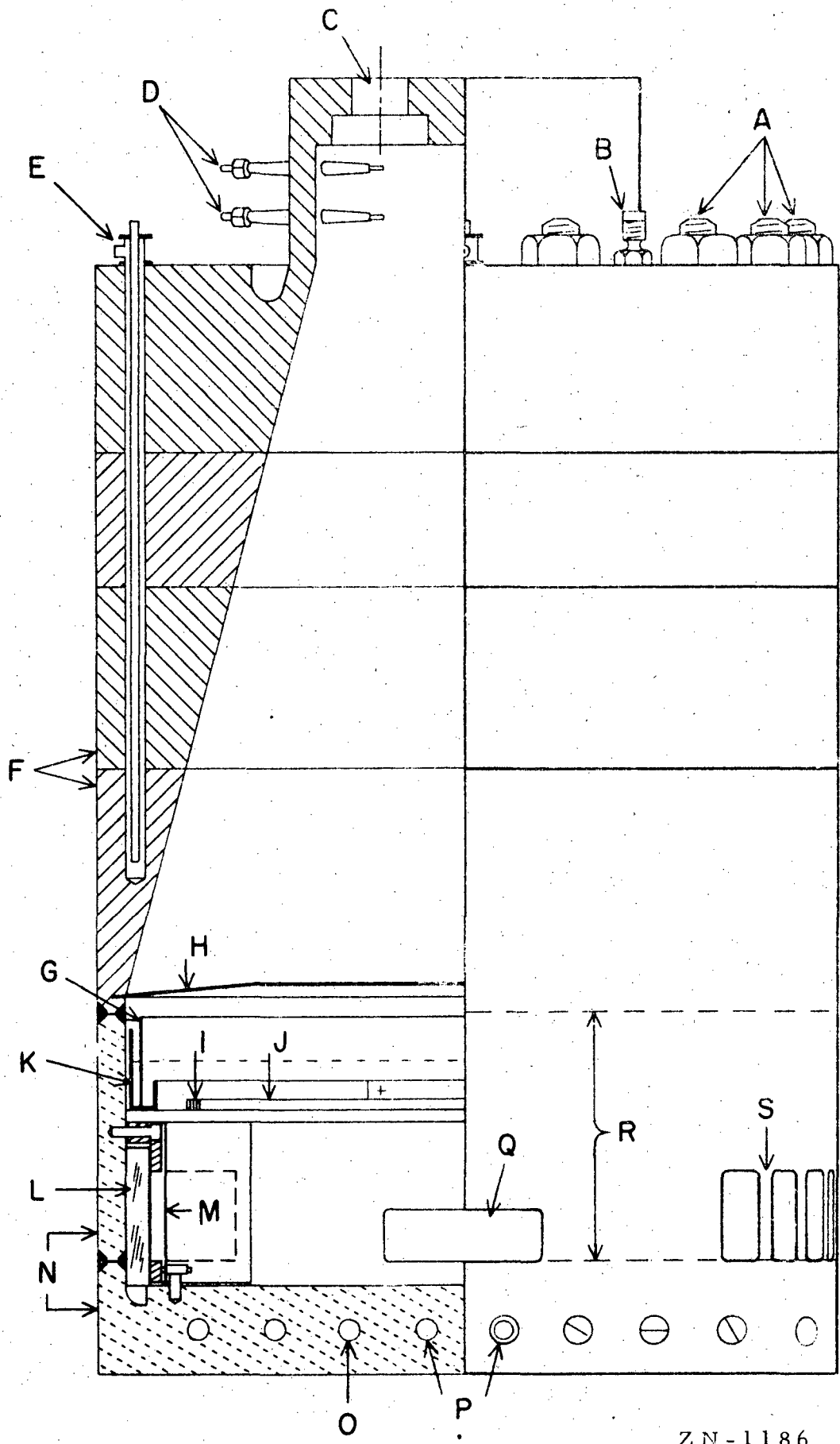
Fig. 1B. Quarter-scale cutaway view of the cloud chamber.

Fig. /.B. Quarter-scale cutaway view of the cloud chamber

    A Stressproof steel main bolts, 1 by 16 inches (16)

    B Pressure line to interior of chamber for gas or alcohol (3)

    C Viewing and camera ports (4)

    D Spark plugs for clearing field and thermocouples (8); no electric heating is used with this chamber at present

    E Squirt tubes (4)

    F Upper pole assembly

    G Wick

    H Black bakelite ring

    I Bakelite clearing-field support

    J Clearing-field wires (5)

    K Copper alcohol tray

    L Cast astrolite windows (2)

    M Homalite heat shield, 1/16-inch

    N Nonmagnetic stainless steel

    O Acetone channel

    P Acetone inlets (2)

    Q Beryllium-copper windows 0.012 x 1.25 x 3 inches (details not shown)

    R Welds

    S Ribs, 3/4 x 1 inch, to support windows L (7 ribs on each side)
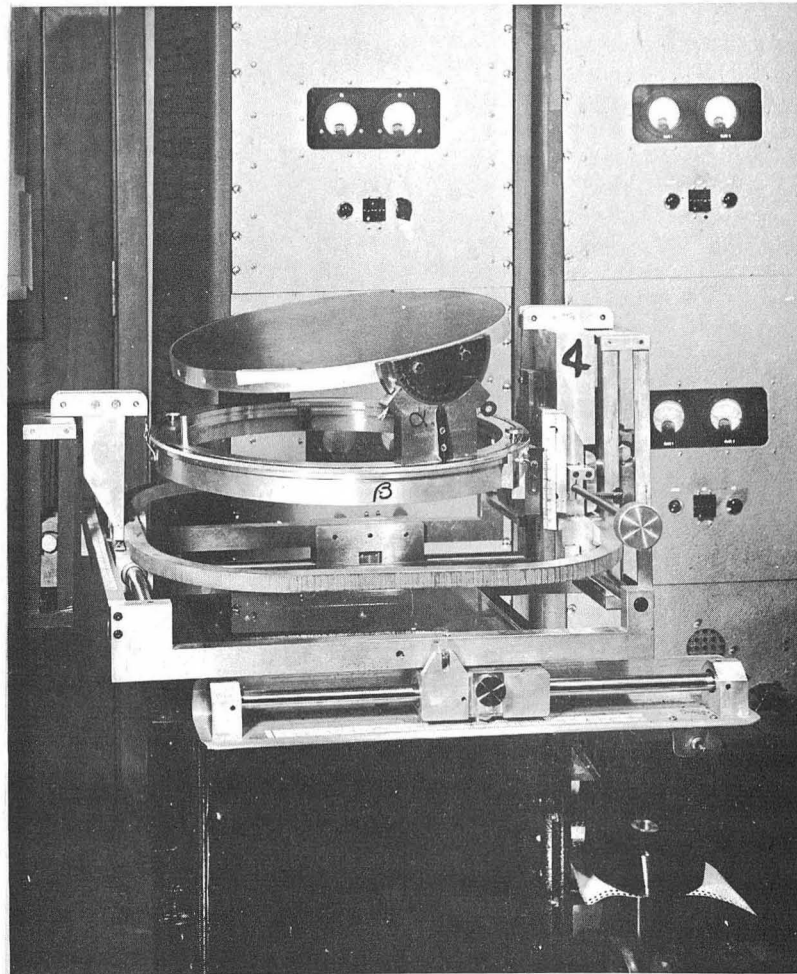
ZN-1528

Fig. 2. The stereoscopic projection apparatus, or "space table."
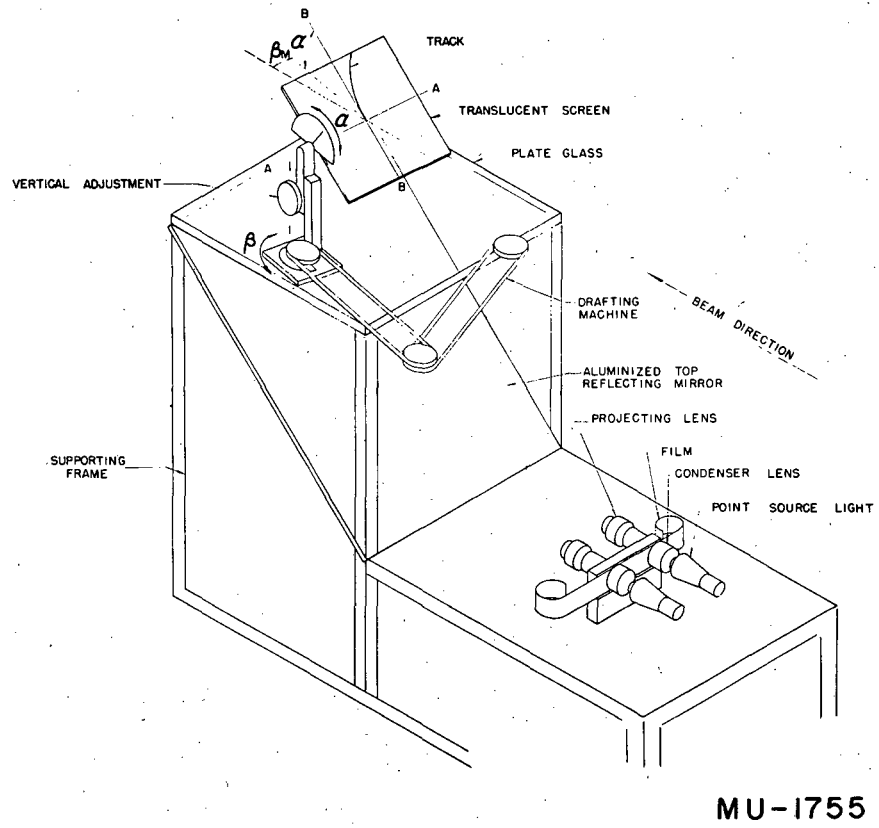
Fig. 3. Schematic drawing of the stereoscopic projection apparatus.

ZN-1529

Fig. 4.   A Λ^0.   The direction of the primary beam is from the top
of the photograph to the bottom.

Dip angle α is the angle between the track and a line vertical to the sensitive-region plane (perpendicular to the beam direction); $\alpha = 0$ points down toward the bottom of the chamber.

Azimuthal angle β is the angle between the projection of the tangent to the track on the horizontal (the plane of the sensitive region) and the beam direction. Thus $\beta = 0$ is the nominal direction of the beam.

In addition, the radius of curvature of the tracks is measured (by matching ruled lucite templates to the track) and the momentum computed from it, the field value, and $\sin \alpha$.

Discussion of Errors

The events were separated into the various types (θ^0, Λ^0, $K_{\pi 2}$, etc.) insofar as possible by use of the curves in Appendix A. This was done prior to machine computations (from which the separation was performed more objectively--see section on Q values, p. 27) as a convenience and as a check on the reliability of the measurements. Any events showing dynamical or ionization inconsistencies were remeasured, and the clearly anomolous decays--that is, those that were not consistent with a known two-body decay mode and Q value--were distinguishable at this point.

The errors listed on the measured variables (Appendix B) are those determined by the measurer to be the values on both sides of (and nearest to) the chosen value that are definitely incorrect. This procedure yields errors, with this equipment, that correspond to approximately one and one-fourth standard deviations for angle measurements and one and one-half standard deviations for radius-of-curvature measurements. This estimate was obtained by examining repeated measurements on a sample group of about fifty prongs. Either two or three sets of measurements were made on each prong and these were tested for consistency, within their stated error, with the means for that prong. From the percentages of measurements that were, and were not, consistent, the equivalent measure stated above in terms of standard deviations was calculated.

Since the incoming particle that produces a V^0 in the chamber wall is not seen, its direction cannot be measured, nor an acceptance criterion established to provide a rigorous error definition for this direction. The error in an assumed beam direction arises from two sources: the inaccuracy of alignment of the measuring device along the assumed direction, and the spread of beam-particle directions about the assumed direction. An estimated standard deviation of $\pm 2^\circ$ in β and $\pm 0.5^\circ$ in α has been placed on the beam direction to account for these uncertainties.

The magnetic field is known to 1.5% as a function of position in the chamber; use of the value at the center of the track for the entire track can, however, cause errors in momentum up to 1.5% (Appendix C). An ammeter recording the magnet current is photographed simultaneously with each chamber picture. From these readings, fluctuations in current are corrected for in the few cases in which they occur.

Motion of the chamber gas causes spurious curvature (as determined from "no field" pictures) nominally of about 100 meters, [18] which is small compared with the measured uncertainties, and is included in the measured estimate of error. At certain times, however, during the experimental runs, this motion became appreciable. The methods of detecting this unusual turbulence were: by eye, in the process of measuring, and by apparent kinematical deviations of the decay from a normal θ^0 or Λ^0 mode. In either case the decay was remeasured, and radius-of-curvature measurements were performed separately on the first and second halves of the track. When these differed, the average was assigned as the measured value, and the greatest and least limits of the two measurements were assigned as the error limits.

This seemed a consistent scheme in that all such affected V^0's, after this procedure, within the limits of error fitted the kinematics of a normal θ^0 or Λ^0 with only one exception. This exception is probably an actual anomalous decay, but was not classed as one, and was left unidentified because of the suspicion of abnormal turbulence.

The pictures were reprojected through an optical system essentially the same as the one in which they were originally taken, in order to minimize optical distortions. The spurious curvatures obtained from the no-field pictures, along with photographs of straight-line grids, indicate that the error from optical distortions is small compared with the measurement uncertainties.

)

Possible Bias Effects

It is necessary to examine the particular features of cloud chambers that may restrict or bias the observations made with them, before passing judgment on the reliability of these observations. To this end, this discussion of several possible causes of bias is included.

Bias Against Vertical Decay and Production Planes

It is common knowledge that V^0 particles with vertical decay planes relative to the plane of the chamber are somewhat more difficult to detect in scanning than those with horizontal decay planes. Also fewer V^0's should be seen with vertical production planes in this experiment, since these pass through the shallow dimension of the chamber. Those with production planes horizontal (parallel to the plane of the chamber) pass through the chamber with a maximum distance in which to decay, therefore more of these should be seen. Figures 5 and 6, which plot the number of Λ^0 and θ^0's vs the production-plane orientation, definitely show this effect. The ratio of V^0's with production planes within 30° of horizontal (or production-plane normals within 30° of vertical) to those with production planes within 30° of vertical is ~2. Deutschmann et al.[32] discuss these two effects (of fewer decays with vertical decay and production planes) with regard to the bias that they may insert in the distribution in angle between production and decay planes, and conclude that they have little, if any, effect on their results. I should like to point out a few additional pertinent factors. In chambers utilizing magnetic fields, in particular those such as the present one with strong magnetic fields, the bias against events with vertical decay planes is not so severe as when there is no magnetic field. The reason for this is that the magnetic field separates the oppositely curving tracks, and the decay has the same appearance as a decay with small opening angle. These are harder to see than wide-angle decays, but the effect is not severe. The ratio of decays within 30° of horizontal to those within 30° of vertical is ~1.1 as compared to the value of 2.0 in the case of the production planes. The magnetic field obviously makes no difference in production-plane bias. (See Figs. 14A and 14B for a plot of the number of events vs the angle of the decay plane relative to the normal to the plane of the chamber.)
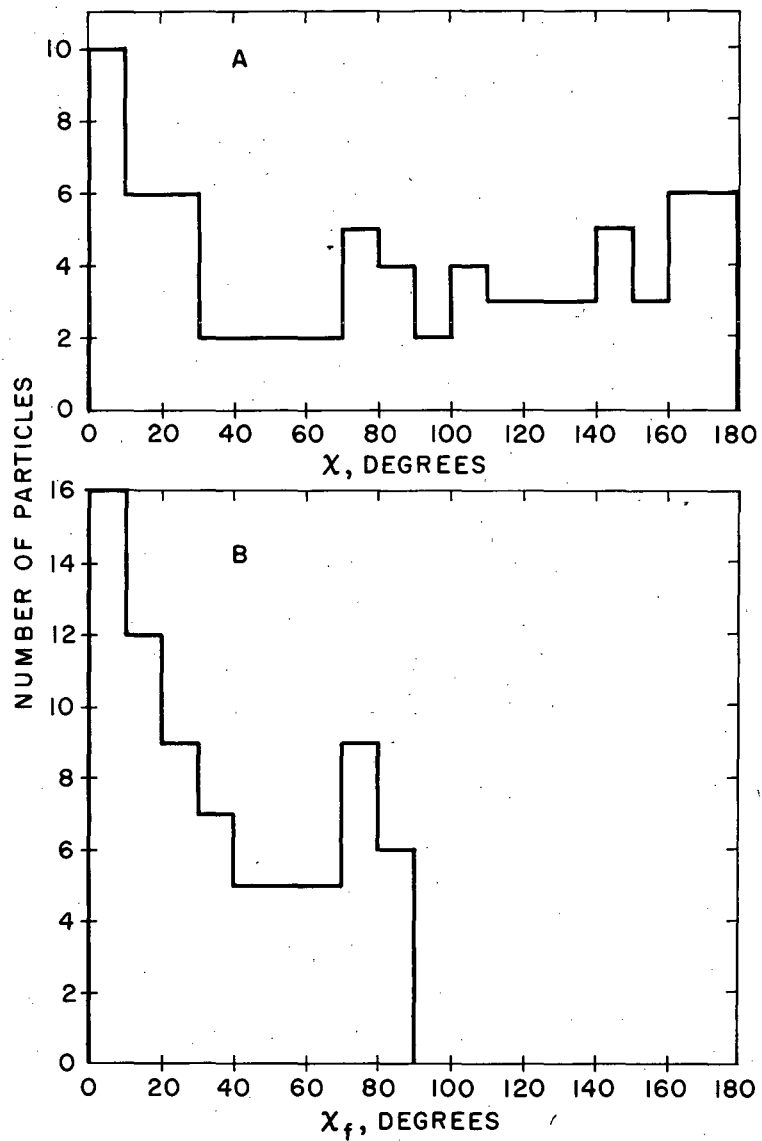
Fig. 5. Λ^0 distribution in production plane orientation χ. B gives this distribution folded into 90°.
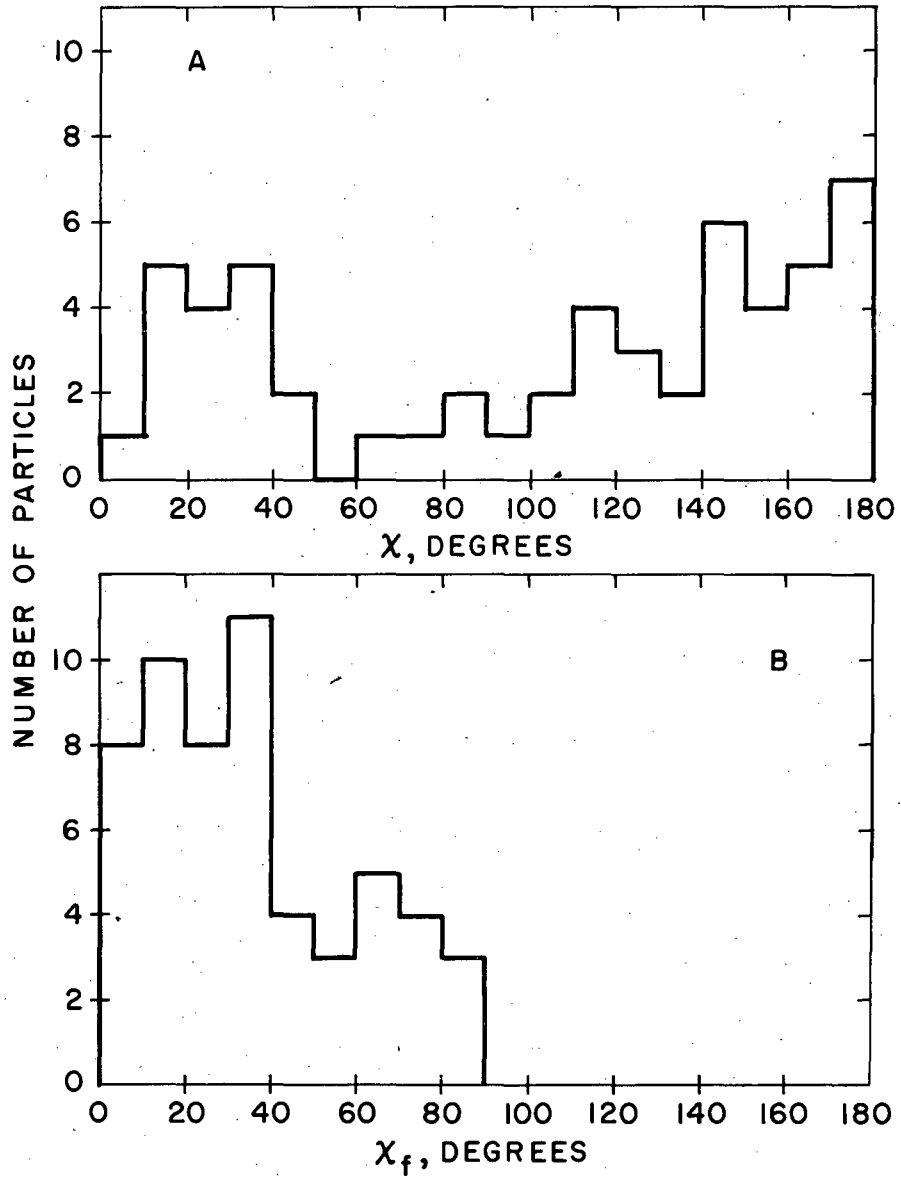
MU-11856

Fig. 6. θ^0 distribution in production plane orientation χ. B gives this distribution folded into 90^0.

MU-11857

Since it is easier to observe V^0's with vertical decay planes in this experiment, it is not surprising to find that my results differ from those of Deutschmann et al. Figure 7A plots the number of Λ^0's having decay planes within 30° of vertical against ϕ, the angle between production and decay planes; Fig. 7B plots the same for the θ^0's. If these nearly vertical V^0's are subtracted from the total distributions in ϕ the result is in essential agreement with the distributions obtained by Deutschmann et al. (See Figs. 12B and 13B; the dotted lines show the distribution after subtracting the nearly vertical decays.)

In order to ascertain whether the bias against vertical production planes affects the distribution in ϕ, the number of V^0's with production plane within 30° of vertical is plotted in Fig. 7C against the corresponding value of ϕ. From the isotropic features of this distribution, I would conclude that the absence of such decays would not distort the complete distribution in ϕ.

Momentum Distribution Bias

This bias, arising from the dependence of the laboratory decay rate on momentum, is discussed under "Detection Efficiency," p. 24.

Bias in Lifetime Determination

In this experiment, as opposed to most cosmic-ray experiments, the origin of the V^0 particle is not seen. Consequently the line of flight cannot be measured directly, but must be calculated from the measured momenta and angles of the decay prongs. This can be done as follows:

$$p_x = (p+) \sin \alpha_+ \cos \beta_+ + (p-) \sin \alpha_- \cos \beta_- ,$$

$$p_y = (p+) \sin \alpha_+ \sin \beta_+ + (p-) \sin \alpha_- \sin \beta_- , \qquad (1)$$

$$p_z = (p+) \cos \alpha_+ + (p-) \cos \alpha_- ,$$

where p_x, p_y, and p_z are the momentum components of the V^0, and the angles α and β are defined on p. 14. From these momentum components, the direction cosines of the line of flight can be computed by formulas such as

$$\cos \alpha_0 = \frac{p_z}{|p|} . \qquad (2)$$

It can be seen from Eq. (1) that these angles of the line of flight are not nearly as accurately determined as the directly measured decay-prong
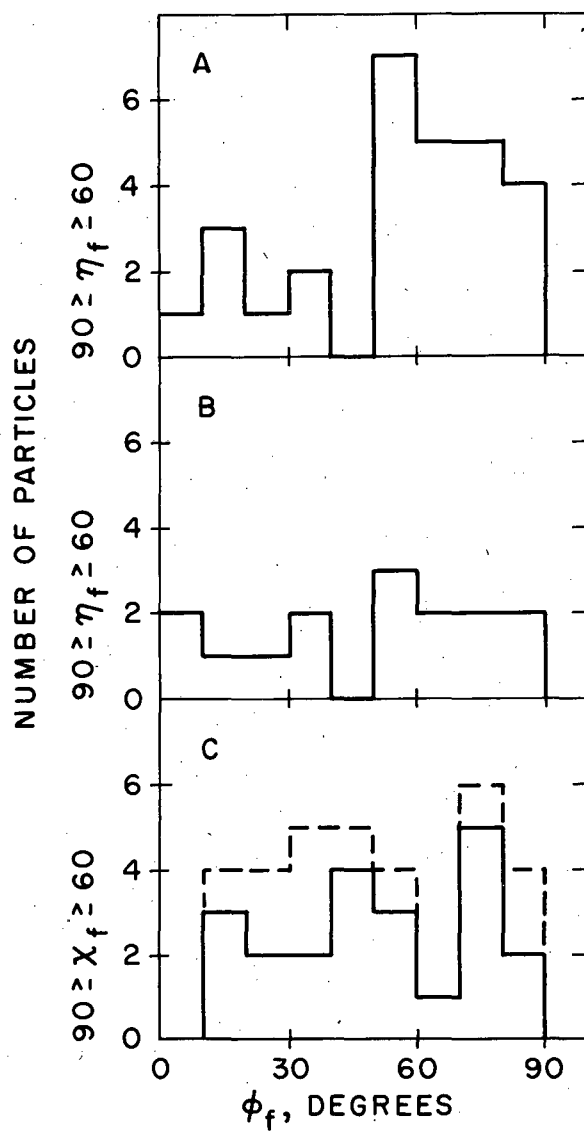
MU-11858

Fig. 7. Distributions in angle ϕ between production and decay
planes. (A) $\wedge^0$'s having decay planes within 30° of vertical.
(B) θ^0's having decay planes within 30° of vertical. (C) V^0's
having production plane within 30° of vertical. Solid line
is for $\wedge^0$'s. The dotted area above the solid line is for θ^0's.

angles, because of the errors (5% to 10%) on p+ and p-. In addition, for values of a_0 close to 90°, the value given by Eq. (2) is virtually meaning-less, within the limits that can be assigned, since p_z can be the difference between two terms of similar magnitudes and rather large errors.

Now, for calculating lifetimes, the distance of travel along the line of flight and the potential distance of travel along the line of flight need to be known. [28] If, as in this experiment, these distances cannot be measured directly, but must be calculated from the position of the decay point in the chamber and the line of flight (or measured along the calcu-lated line of flight), then the dependence of the potential path-length cal-culation on terms such as in Eq. (2) renders the result very unreliable (the measured distance along the line of flight is subject to the same un-reliability). For this reason it does not seem advisable to perform mean lifetime computations for the work reported here. Further reason is provided in that in the diffusion chamber the sensitive volume is not as well defined as in the expansion chamber, and it is therefore more diffi-cult to establish reliable fiducial planes from which to measure the needed distances (when the origin is not seen).

Charged-V Scanning Bias

Charged V's are more difficult to find in scanning cloud-chamber photographs than neutral V's, since their geometric form departs less from that of the background. The number of charged V's obtained in these experiments is too small to compute an efficiency factor, or an estimate of this bias effect; however, since only qualitative comparisons for charged V's are considered herein, this bias need not be taken into consideration.

Wide-Angle V^0's

Gayther and Butler[29] take into account the biasing effect, in their experiment, of their inability to see V^0's produced in the angular region close to 90° (taken with reference to the direction of the incoming beam or initiating particle). This occurs because of the presence of lead plates in their chamber, and is an important consideration, since at the energies involved in their experiment V^0's are produced in much the same quantities over all directions from 0° to 180°. In the experiment reported here the cloud-chamber wall serves a purpose analogous to that of their lead plates, and would be subject to the same bias if wide-angle V's were

produced in the energy range involved. However, from the angular distributions obtained (see Figs. 5 and 6), it can be seen that practically all the V^0's lie within 25° of the incoming beam direction. Hence a possible bias against wide-angle V^0's need not be taken into account.

Although the presence of V^0's emitted in the backward direction in the laboratory cannot be ascertained for collisions in the front wall of the chamber, it can for collisions in the far wall, and none of these were seen. Very low-energy V^0's, however, which these would tend to be, could all decay in the insensitive region near the wall of the chamber and would be missed.

Center-of-Mass Emission-Angle Bias

It should be noted, in determining the relative frequency of forward proton (π^+) emission in the center-of-mass system of the Λ^0 (θ^0), that the indistinguishable V^0's influence this result. This follows from the fact that in the region of phase space where the Λ^0 and θ^0 dynamical parameters overlap (and the Λ^0's and θ^0's cannot then be distinguished kinematically), the proton always goes forward for the Λ^0, and the π^+ goes forward for the θ^0. (This can be seen from Fig. 22 in Appendix A.)

Thus if the true frequencies are random forward and backward, one would expect an excess of backward protons in the distinguishable Λ^0's and backward π^+ for the θ^0's. Actually these data yield an excess of forward π^+ for the θ^0, and consequently this excess is augmented by the indistinguishable cases. These results are discussed further in the section on center-of-mass emission angles, p. 38.

This effect might also lead to a systematic difference between the observed CMS emission angle distribution and the true distribution. From Fig. 22 in Appendix A it can be seen that the locus of indistinguishable phase-space points is approximately along $p_+ \cong 6p_-$. Also along this locus we have $p_1 \cong 0.104/\sin\theta$. Inserting these into $\sin\theta_{CMS} = \dfrac{p_1 p_2 \sin\theta}{p + P}$ yields, for Λ^0, $\sin\theta_{cms} \cong \dfrac{1.82}{\sqrt{3.08 + \cos\theta}}$; θ_{CMS} is the angle between the direction of emission of the π^- and the line of flight of the V^0, in the center-of-mass system of the decay. In the angular range 0° to 60° the denominator varies only from about 1.9 to 2.0. Inserting 1.95, we have

$$\sin\theta_{CMS} \cong 0.933 ,$$

$$\theta_{CMS} \sim 69^\circ .$$

A diminuition in the number of distinguishable Λ^0 decays in the vicinity of this angle might be accounted for on this basis. The corresponding angle for θ^0's is $\sim 27^\circ$.

Gas-Produced V's

Among the V's stated here as being produced in the wall, there are undoubtedly some that were actually produced in the chamber gas. The point of production in such cases is in an insensitive "hole" in the sensitive volume, or just outside the sensitive volume. Lower-energy V's, which normally decay close to their point of production and would not be seen in this chamber otherwise, would be observed from unseen gas interactions. The effect of these gas-produced V's is small because their number is small compared to the wall-produced ones, except where calculations involving the chamber detection efficiency (see p. 24) are made. If decays are weighted inversely as their detection probability, low-momentum decays have large weights. Distributions or quantities involving low-momentum decays would then be distorted by the large weights assigned to these gas-produced, low-momentum V's. For these reasons, the cross-section estimates, momentum distributions, and branching ratios given in this report are made subject to low-momentum cutoffs. These are stated explicitly with the pertinent results.

Detection Efficiency

Since the laboratory lifetime of an unstable particle depends on its energy, the number that decay over a given length traversed in space depends on their energy also. This has been expressed analytically by Gayther and Butler,[29] who derived a detection probability

$$P(t, T) = e^{-t/T_0} - e^{-T/T_0} ,$$

where t is the time of flight from the point of production of the particle to the point in the chamber where it can just be observed and measured, and T is the maximum total time of flight it could have in the chamber if it did not decay (also measured from the point of production) and still be observed and measured. Substituting the minimum and maximum distances for the 36-atmosphere chamber that determine t and T, we have

$$P_i(p) = e^{-a_i/p} - e^{-b_i/p} ,$$

$$i = 1, \theta^0, a_1 = 2.177, b_1 = 6.063 ,$$

$$i = 2, \wedge^0, a_2 = 1.000, b_2 = 2.786 ,$$

$$i = 3, \Sigma^-, a_3 = 10.57, b_3 = 29.45 ..$$

These formulae are written for p measured in Bev/c, and are plotted in Fig. 8. They are valid for V^0's traversing the chamber with lines of flight near the horizontal. Following Gayther and Butler, the weight $W = 1/P(p)$ should be assigned to each decay, and this, then, corrects for the V's that decay before entering or after leaving the chamber. These weights are used in calculating the momentum distributions (see Figs. 16 through 21) and the total number of V's that pass through the chamber. The value of W for each V^0 analyzed is listed in column 12 of Appendix B. The errors shown are standard deviations, calculated according to the recipe given by Gayther and Butler. This analysis assumes that all the V^0's are horizontal, which is not strictly true, but should be a useful approximation on account of the forward-peaked laboratory angular distributions.
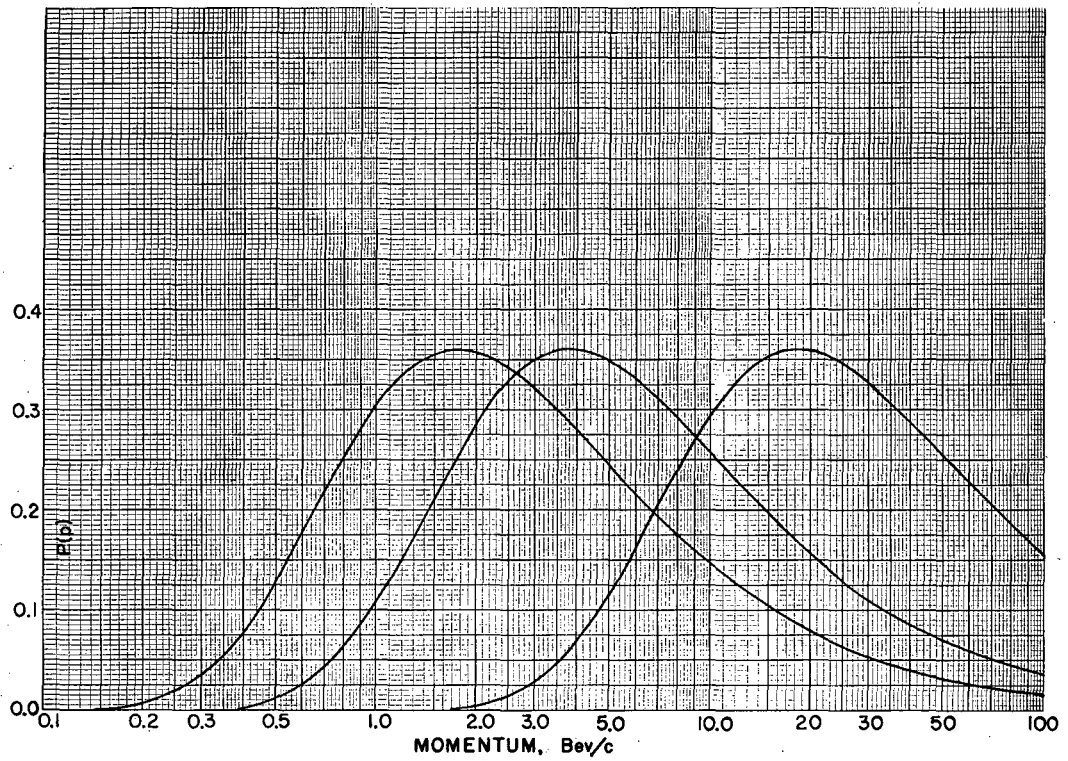
Fig. 8. Detection efficiency of the 36-atmosphere cloud chamber. The ordinate P(p) is the probability of detection.

Scanning Efficiency

Defining "scanning efficiencies" e_1 and e_2 for two scanners by the formulae

$n_1 = e_1 N$ = no. of events found by scanner #1,

$n_2 = e_2 N$ = no. of events found by scanner #2,

$n_{1,2} = e_1 e_2 N$ = no. of events found by scanners #1 and #2

(N is the "true" number of events),

one can crudely estimate the number of missed events. In my work these equations gave, for the two least experienced scanners, $e_1 = 0.75$ and $e_2 = 0.97$, when applied to the film that they scanned independently. Since all the film was scanned either by these two scanners, or by more experienced scanners, and since much of it was scanned three times instead of two, this estimate would indicate a negligible proportion of missed V^0 decays.

III. RESULTS AND DISCUSSION

Q Values and Identification Procedure

The mean Q values, the energy released in the act of decay, with standard deviation of the means calculated according to

$$\sigma = \left[\frac{(Q - \bar{Q})^2}{n\,(n - 1)}\right]^{1/2} , \text{ are}$$

$$Q(\Lambda^0) = 40.2 \pm 0.9 ,$$
$$Q(\theta^0) = 220.5 \pm 5.1 .$$

Histograms of the Q-value distributions are shown in Figs. 9A and 9B. These plot the number of Λ^0's and θ^0's against Q. The standard deviations of these distributions are 6.7 and 32.9 Mev, respectively. These compare quite favorably to the nominal internal errors on the Q values, which are 8 Mev and 40 Mev (Appendix B), as these latter figures have been estimated independently as about 1.5 standard deviations (see Section on error, p. 15).

For those completely measurable decays that ionization does not unambiguously identify, Q values assuming θ^0 identity ["$Q(\pi^+, \pi^-)$"] and Q values assuming Λ^0 identity ["$Q(p^+, \pi^-)$"] were calculated. A decay was than classed as a Λ^0 if $Q(p^+, \pi^-) \pm \delta Q$ included 37 Mev, and if $Q(\pi^+, \pi^-) \pm \delta Q$ was different by two error intervals or more (approximately three standard deviations) from 214 Mev; and vice versa for the θ^0. Those completely measurable decays that do not satisfy this classification were then classed as indistinguishable if the Q values calculated were consistent, within the two error intervals, with both θ^0 and Λ^0 identities. They were classed as anomalous if the Q values were inconsistent with both identities and the photograph showed no apparent distortive features, and were classed as unidentifiable if the Q values were inconsistent with both identities and some distortive features were apparent. The 45 decays that were found indistinguishable by the above criteria were not included for analysis, and consequently all results contain the implicit assumption that these cases do not bias the results (except for CMS emission angles: see sections on center-of-mass emission angle bias and CMS emission angles, p. 22 and 38).

Those decays observed that were only partially measurable were occasionally identifiable by ionization or by a discriminating lower limit on the badly determined prong. This type of analysis was performed
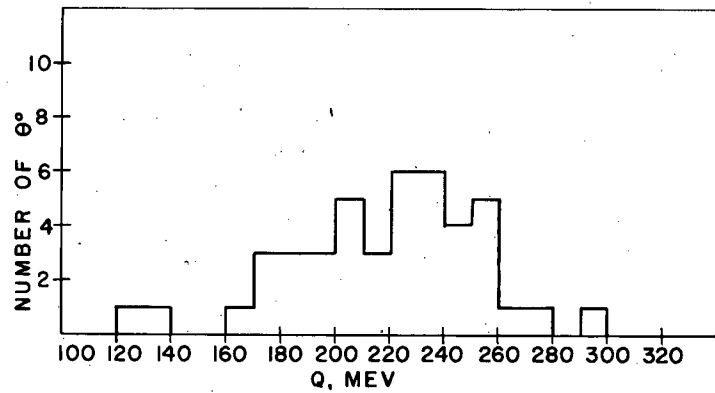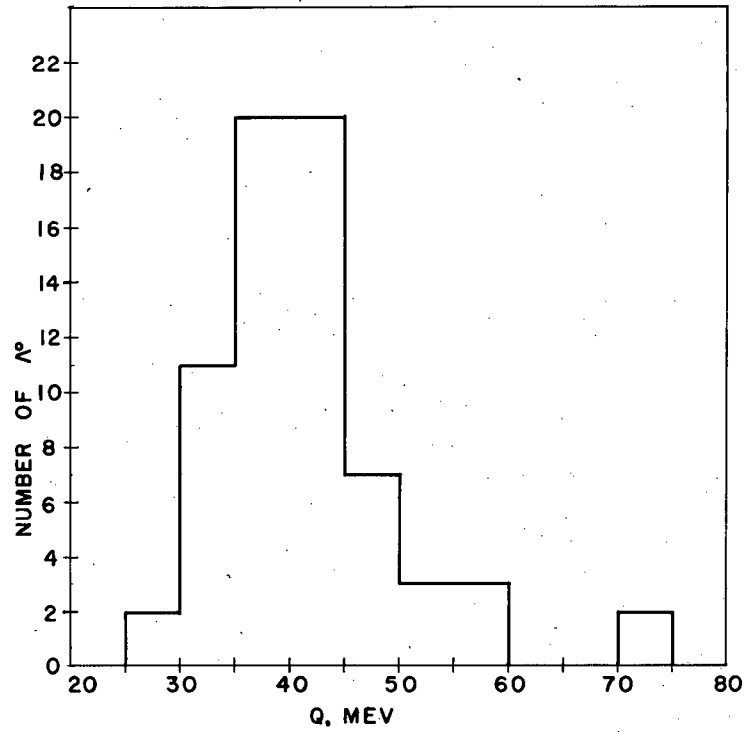
Fig. 9. Q-value histograms. A. For Λ^0. B. For θ^0.

MU-11860

with the curves of Appendix A, and a value of momentum assigned to the badly determined prong from the curves where the lower limit or ionization definitely discriminated. V^0's identified in this fashion, with the assigned momentum, were then included in all distributions and calculations except in the mean Q-value determinations. The partially measurable cases, which could be either θ^0's or Λ^0's, were classed as unidentifiable, except those for which the assigned momentum was the same for both identities. These were classed indistinguishable.

The dynamic characteristics of all the completely measurable V^0 decay events are listed in Tables VII, VIII, and IX of Appendix B. Table I, below, lists the identification classification of all V^0's obtained for the three primary beams. Table II gives the weighted number (corrected for detection efficiency) of Λ^0, θ^0, and indistinguishable V^0's. For the indistinguishable V^0's, the smaller of the two possible weights is assigned, making the given weighted number a lower limit. Because of the effect of gas-produced V's whose origins are not seen (p. 23), these weighted numbers are restricted to Λ^0 with $p \geq 0.5$ Bev/c, θ^0 with $p \geq 1.0$ Bev/c, and indistinguishables with $p \geq 0.5$ Bev/c.

Table I

Relative numbers of V's produced in the various primary Bevatron beams. All those in a single column were produced by the same incident flux.

	Primary Bevatron beam		
	π^- 4.5 Bev/c	n 0 to 7.2 Bev/c	p 6.2 Bev/c p
Identified Λ^0	41	30	7
Identified θ^0	39	17	4
Indistinguishable	19	17	9
Anomalous	1	3	0
Unidentifiable	3	19	3

Table II

Relative numbers of V's weighted for the chamber detection
efficiency. Only those θ^0's are included for which $p \geq 1.0$ Bev/c,
Λ^0's for which $p \geq 0.5$ Bev/c, and indistinguishables for which
$p \geq 0.5$ Bev/c.

| | Primary Bevatron beam | | |
	π^-	n	p
Λ^0	132 ± 20	96 ± 18	25 ± 10
θ^0	161 ± 28	44 ± 13	6 ± 6
Indistinguishable	55 ± 13	54 ± 14	26 ± 9

Cross Section for V^0 Production

Only a rough estimate of the production cross section can be made, because of the irregular thickness of the front of the chamber, which serves as target, and the inability to identify all V^0's as either θ^0 or Λ^0. As the two particles have different detection probabilities in the chamber, the indistinguishable cases cannot be assigned a correct weight to account for those which do not decay in the chamber. By assigning the larger of the Λ^0 - θ^0 detection efficiencies (the smaller weight) in the indistinguishable cases, by dividing the total weighted number of such cases in the same proportion of Λ^0's to θ^0's as the identifiable cases, and by taking an average thickness of the front of the chamber, one can make an estimate of the π^- - p production cross section. The result is, for Λ^0's having momentum $p \geq 0.5$ Bev/c, and θ^0's having $p \geq 1.0$ Bev/c:

$$\sigma(\pi^- - p, \Lambda^0) = 0.12 \text{ mb}, \quad p(\Lambda^0) \geq 0.5 \text{ Bev/c} ;$$

$$\sigma(\pi^- - p, \theta^0) = 0.15 \text{ mb}, \quad p(\theta^0) \geq 1.0 \text{ Bev/c} .$$

The presence of neutron contamination in the proton beam used precludes a reliable estimate for proton production.

Production Angular Distributions

Figures 10A and B give the relative differential cross sections for Λ^0 and θ^0 production in the laboratory frame of reference. Here α' is the polar angle relative to the beam direction. Figures 11A and 11B are histograms of the angular distributions of Λ^0's and θ^0's in the assumed center-of-mass production system for those made in the pion beam--that is, the center-of-mass system of a 4.5-Bev pion and a nucleon. The Λ^0's seem to be emitted predominantly in the backward direction and the θ^0's in the forward direction. Here Ω is the angle between the emitted V^0 and the line of flight of the incident pion.
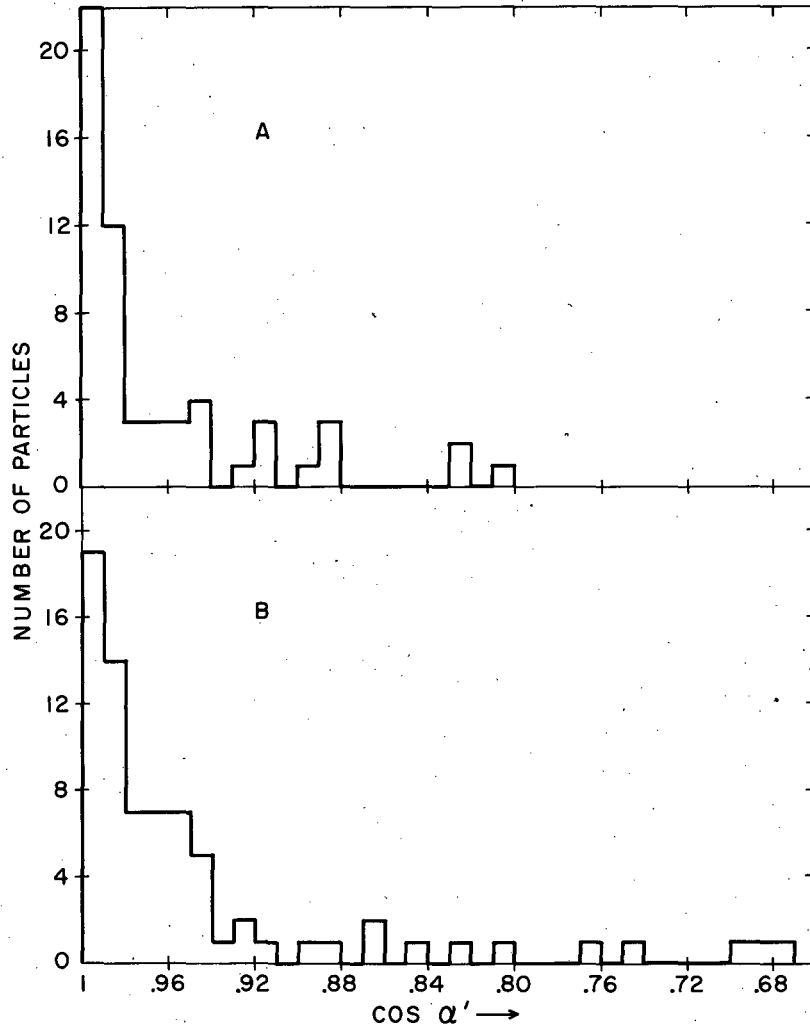
Fig. 10. Laboratory angular distributions of (A) θ^0's and (B) Λ^0's. Here α' is the polar angle between the line of flight of the V^0 and the direction of the incident beam.
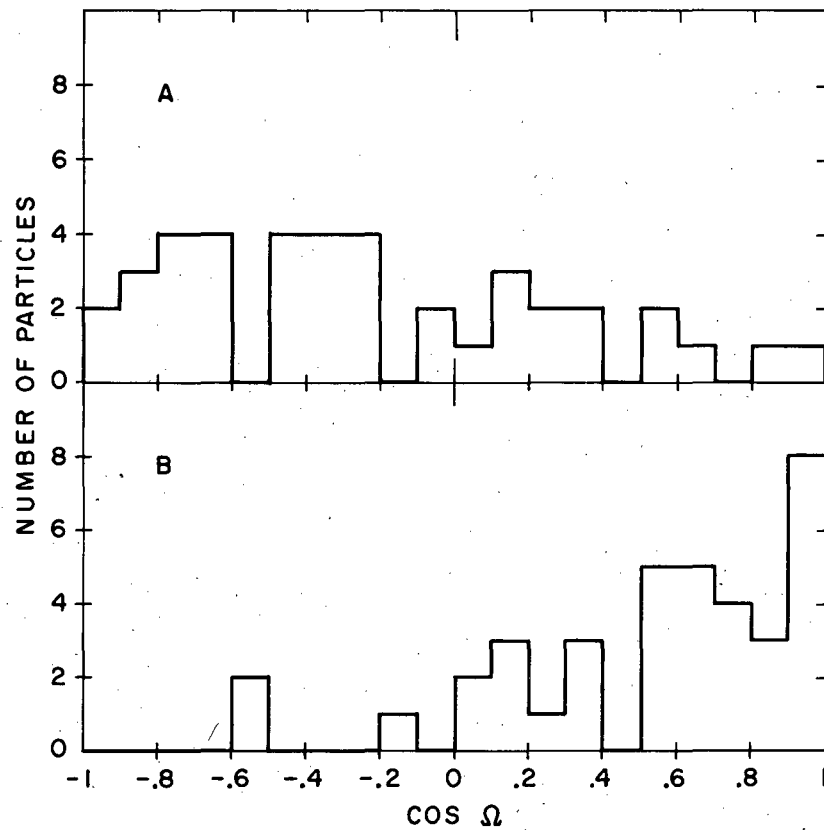
MU-11862

Fig. 11. Angular distributions of (A) Λ^0's and (B) θ^0's in the center of mass of the production system. Here Ω is the angle between the emitted V^0 and the line of flight of the incident pion.

Possible Spin Effects on V^0 Decay Features

Treiman and Wyld[27] and Treiman, Reynolds, and Hodson[27A] have shown that a possible consequence of a spin greater than 1/2 for the Λ^0 (or spin greater than 0 for the θ^0) would be an anisotropy in the distribution in the angle between the production and decay planes of V^0's (this angle is called ϕ in this report). Indications of angular correlations of this type, which might yield information on the spin of the Λ^0, were first noted by Fowler et al.[4] in the analysis of the first Λ^0's from π^- - p collisions, obtained in experiments carried out with the Brookhaven Cosmotron. Subsequent work has not yet been decisive as to whether such correlations (or others) exist. Consequently this section is devoted to the angle ϕ, and to other distributions that might be influenced by spin. The effects, on possible correlative features, of nucleon motion in the nucleus (in which a V^0 is produced), of double collisions within the parent nucleus, and of a possible magnetic-moment precession, are discussed in Appendices D, E, and F, respectively. These discussions indicate that these effects, though not negligible, would not be expected to completely destroy possible angular correlations at the energies of production used in this study.

Distribution of Angle Between Production and Decay Planes

The distributions obtained for Λ^0's and θ^0's are shown in Figs. 12A and B and 13A and B. The gross features are consistent with the symmetry about 90° that conservation of parity would lead one to expect. The ratio of decays with $\phi < 90^\circ$ to those with $\phi > 90^\circ$ is 1.3 ± 0.3 for the Λ^0's and 0.7 ± 0.2 for the θ^0's. Figures 12B and 13B show the full distribution (0° to 180°) folded into the region 0° to 90° for comparison with other experimental data where either the folding has been performed or the experiment did not distinguish between the positive and negative prongs of the V^0. The folded (0° to 90°) angles are labeled with a subscript f.

These distributions are within the allowable fluctuations of isotropy, and do not seem to show the small-angle preferences that has been found by some other experimenters. The dotted lines in Figs. 12B and 13B show the distributions in ϕ after those decays with nearly vertical decay planes (within 30° of vertical) have been subtracted out. The
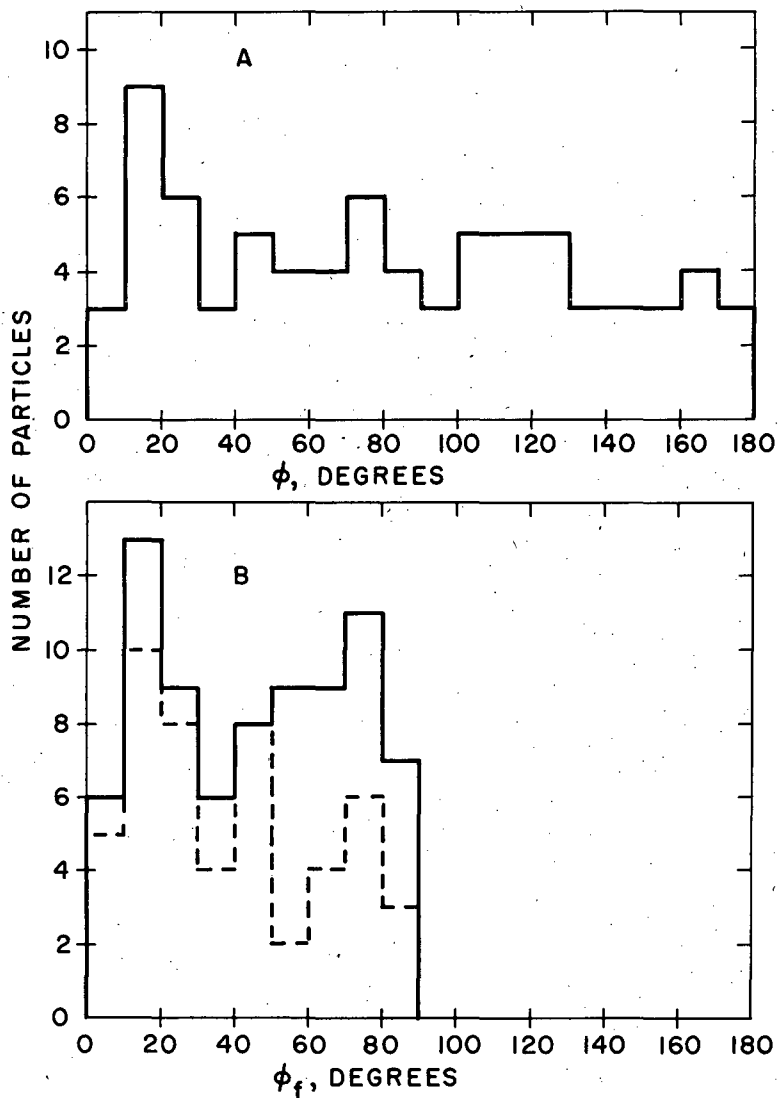
Fig. 12. Λ^0 distribution in angle ϕ between production and decay planes. In B the distribution has been folded into 90°.
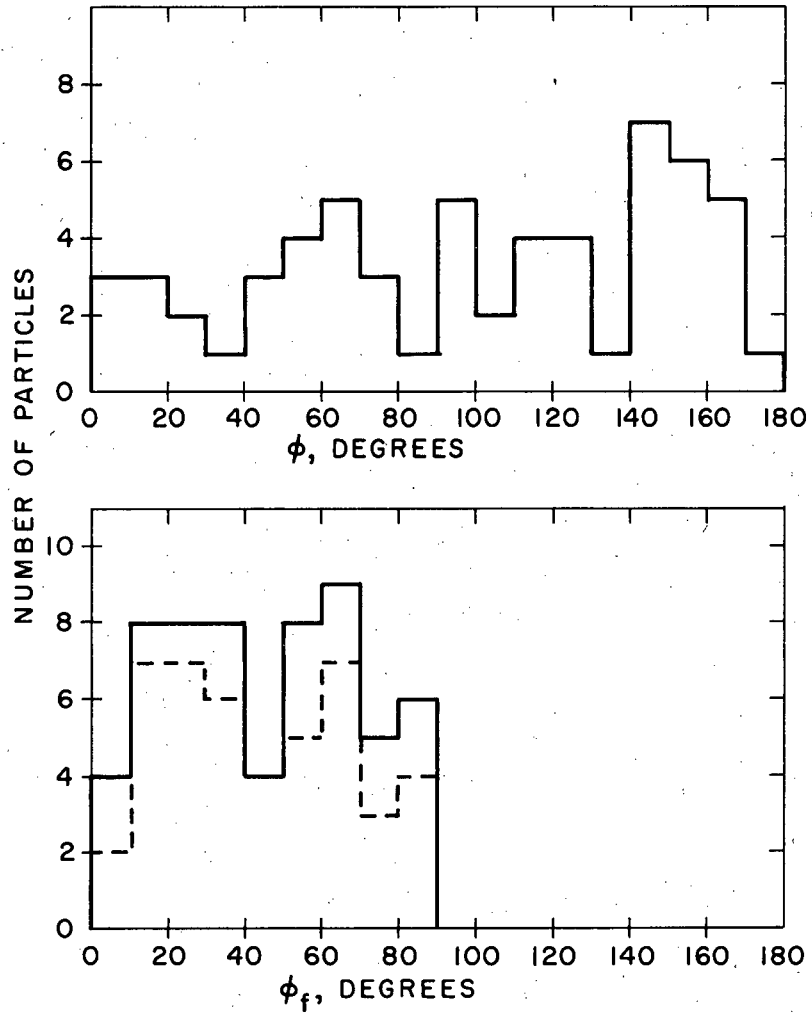
Fig. 13. θ^0 distribution in angle ϕ between production and decay planes. In B the distribution has been folded into 90^0.

dotted distributions, particularly the Λ^0, do show a small-angle preference. Consequently experiments in which this type decay are biased against and missed may be expected to show this small-angle preference. It is interesting to note the two peaks that occur in the Λ^0 decay-plane distribution, Fig. 14A (Fig. 14B gives this distribution over the entire angular range 0° to 180°; Figs. 14C and 14D give the decay-plane distribution for the θ^0's). These peaks seem to indicate a tendency of the Λ^0 decay planes to line up with respect to the magnetic field along two preferred directions. Since the statistics are poor, however, this conclusion cannot be drawn with certainty.

Center-of-Mass Emission Angles Relative to the Line of Flight

Figures 15A and 15B are histograms of the distributions in emission angle in the center-of-mass system of the V^0. The angle calculated is that of the negative decay product relative to the line of flight. The ratio of backward to forward protons for the Λ^0's is 3.5 ± 1.0. For the θ^0, the ratio of forward π^+ to backward π^+ is 1.25 ± 0.33. Before interpreting these results, one must consider the class of "indistinguishable" V^0's. To be dynamically equivalent, a θ^0 and a Λ^0 must both have forward positive decay products, so that failure to include these cases biases the ratios just given. Including them would increase the relative number of forward protons. This indicates that the forward-backward asymmetry of these results for Λ^0's may not be a real one. (In order for the ratio to be unity, however, 90% of the indistinguishables would have to be Λ^0's.) The situation is different for the θ^0's, since the addition of the θ^0's that are among the indistinguishables can only tend to increase the asymmetry. I would conclude that either an unusually small percentage (10% or less) of the indistinguishables are θ^0's, or that the asymmetry is bona fide.

Emission of Decay Products Relative to Production Plane

The ratio of negative mesons decaying upward in the production plane to those decaying downward has been calculated. Calling this ratio Rp, we have

$$Rp\ (\Lambda^0) = 1.05 \pm 0.3\ ,$$

$$Rp\ (\theta^0) = 1.08 \pm 0.3\ .$$

There is no evidence of nonuniformity.
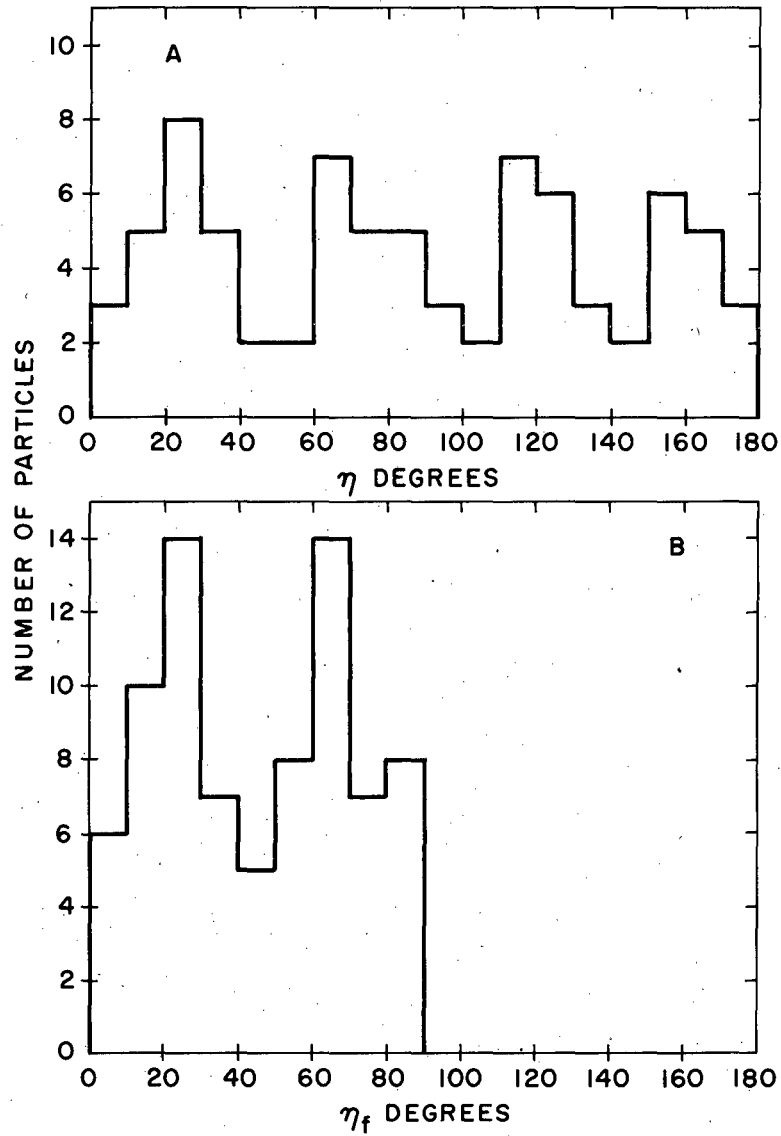
Fig. 14A, B. Λ^0 decay plane distribution. In B this distribution
is shown folded into 90°.
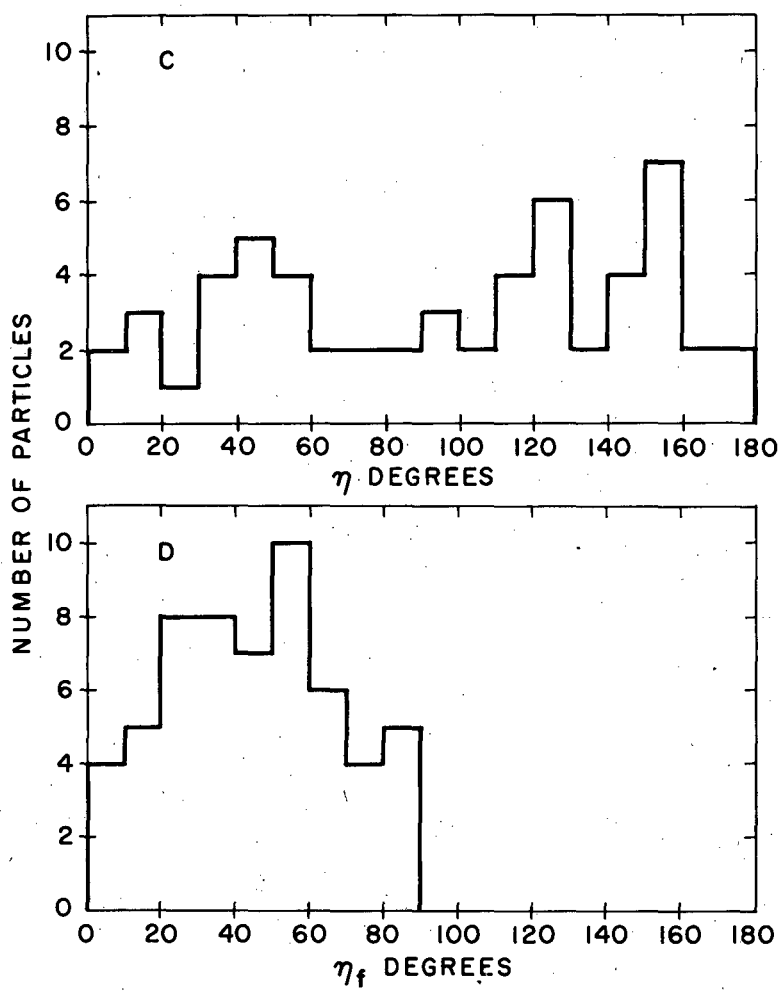
MU-11865

Fig. 14C, D. θ^0 decay plane distribution. In D this distribution is shown folded into 90°.
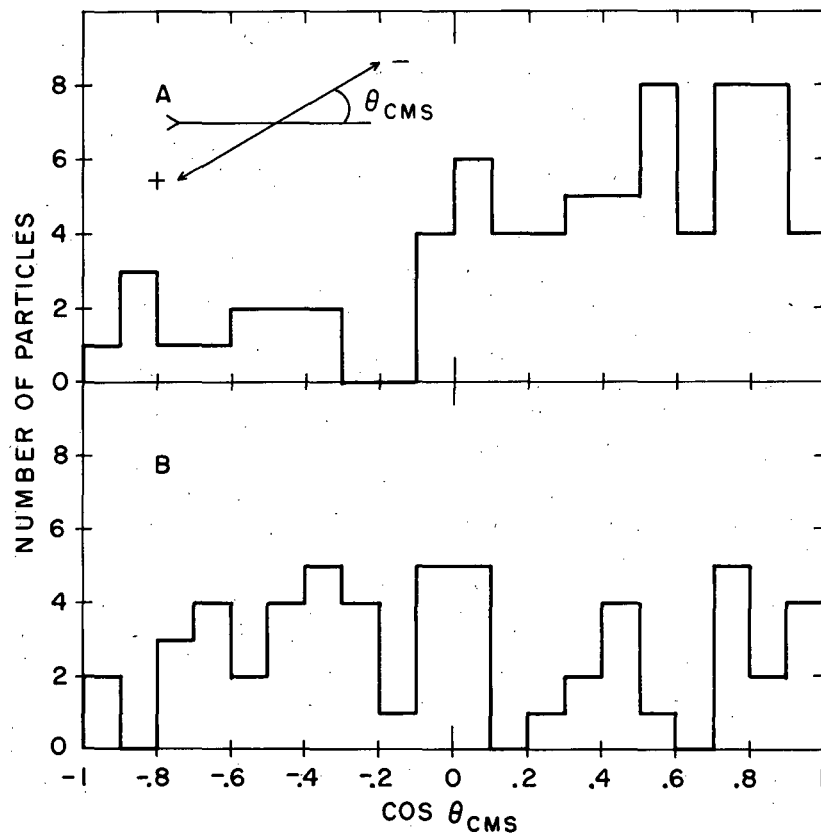
Fig. 15. Distribution in center-of-mass emission angle of the π^- relative to the line of flight (A) for Λ^0's and (B) for θ^0's.

MU-11867

Momentum Distributions at Production

For reference, the momentum distribution of all the Λ^0 and θ^0 is plotted in Figs. 16 and 17. Since these have been produced at different energies by different particles, the more interpretable separate distributions, Figs. 18, 19, 20, and 21, are given. These give the distribution in momentum (Bev/c) of V^0's produced by 4.5-Bev/c pions and by neutrons with $p \leq 7.2$ Bev/c, respectively. These distributions have been corrected for the detection efficiency of the chamber by weighting each event actually observed inversely as its probability of detection. (See p. 24.) Thus each distribution represents the number of V^0's passing through the chamber, rather than the number decaying in the chamber.

Theoretical calculations of such distributions have been made by Jastrow[34] for energies up to 500 Mev. Should these calculations be extended into the Bev range, a comparison could be made with the data presented here.

These distributions are not given for the proton-produced V^0's because of the presence of neutron contamination in the beam. The graphs cut off on the lower momentum side at 0.5 Bev/c for Λ^0 and 1.0 Bev/c for θ^0, because of the distorting effect of gas-produced V's (see p. 23).
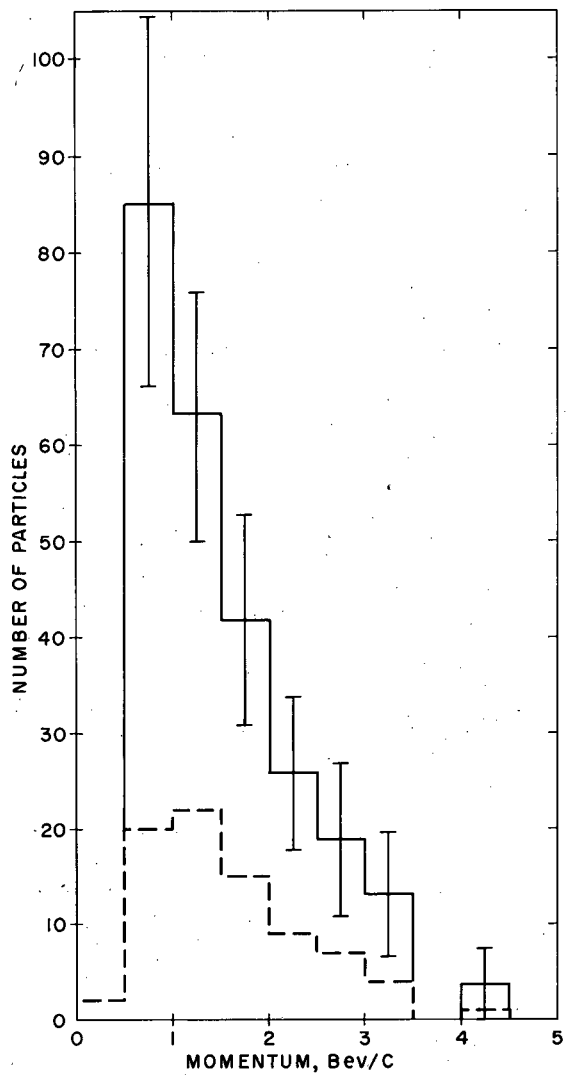
Fig. 16. Momentum distribution of all $\wedge^0$'s. The dotted line shows the actual number of $\wedge^0$'s, the solid line shows the weighted (for detection efficiency) number.
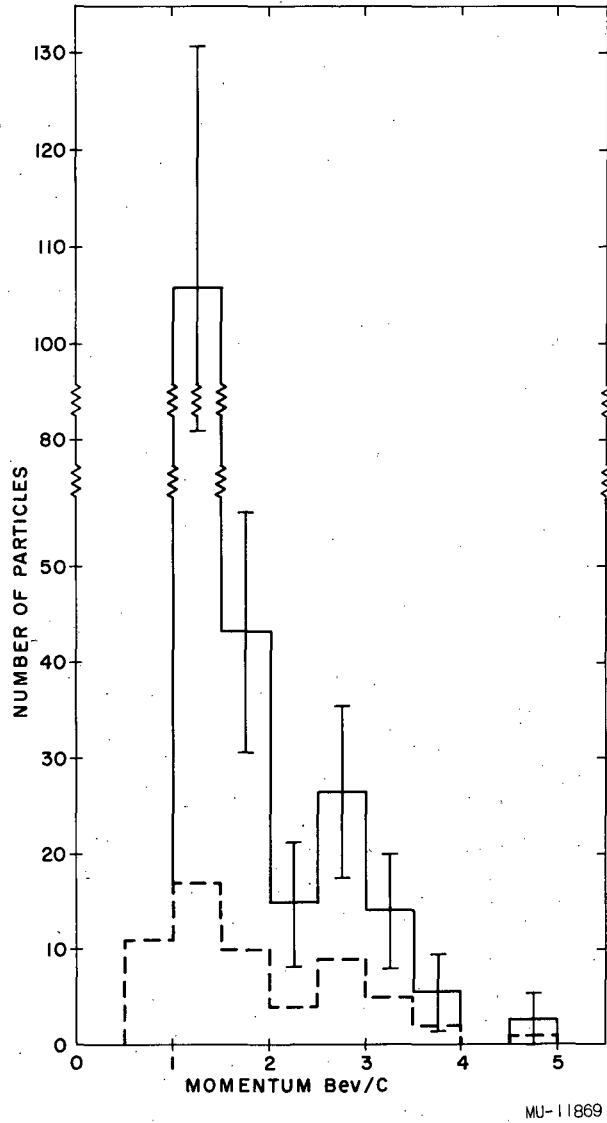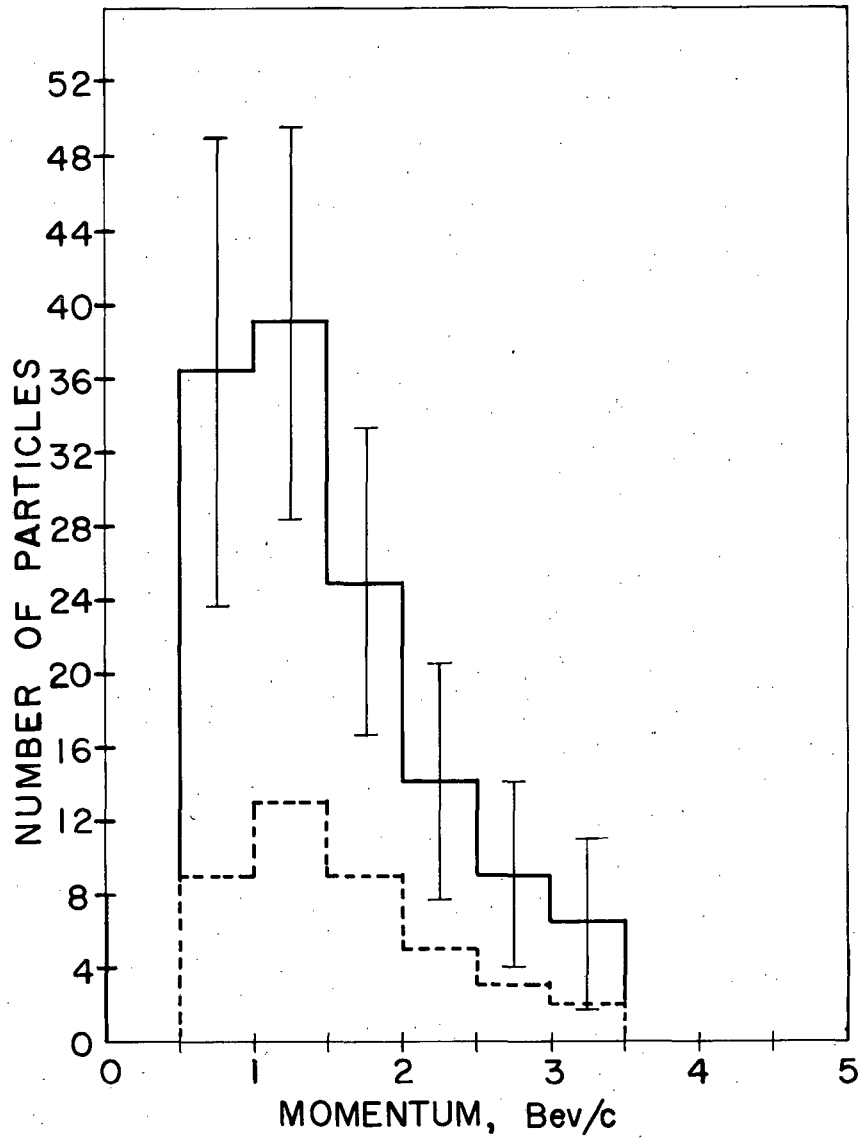
Fig. 17. Momentum distribution of all θ^0's. The dotted line shows the actual number of θ^0's, the solid line shows the weighted (for detection efficiency) number.

Fig. 18. Momentum distribution of Λ^0's produced by 4.5-Bev/c π^- mesons. The dotted line is the actual number, the solid line is the weighted number of Λ^0's.

MU-11870

NUMBER OF PARTICLES
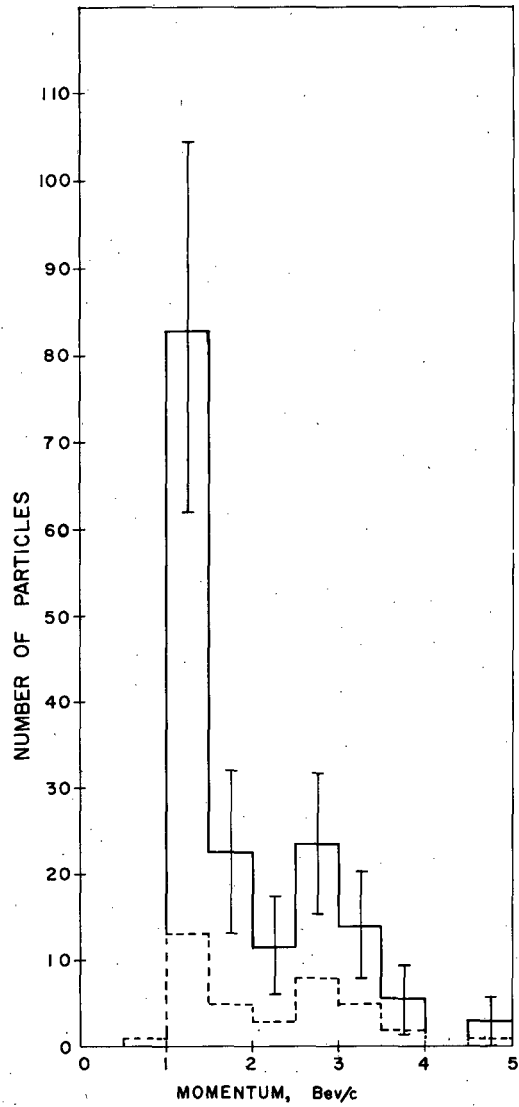
MOMENTUM, Bev/c

MU-11871

Fig. 19. Momentum distribution of θ^0's produced by 4.5-Bev/c π^- mesons. The dotted line is the actual number, the solid line is the weighted number of θ^0's.
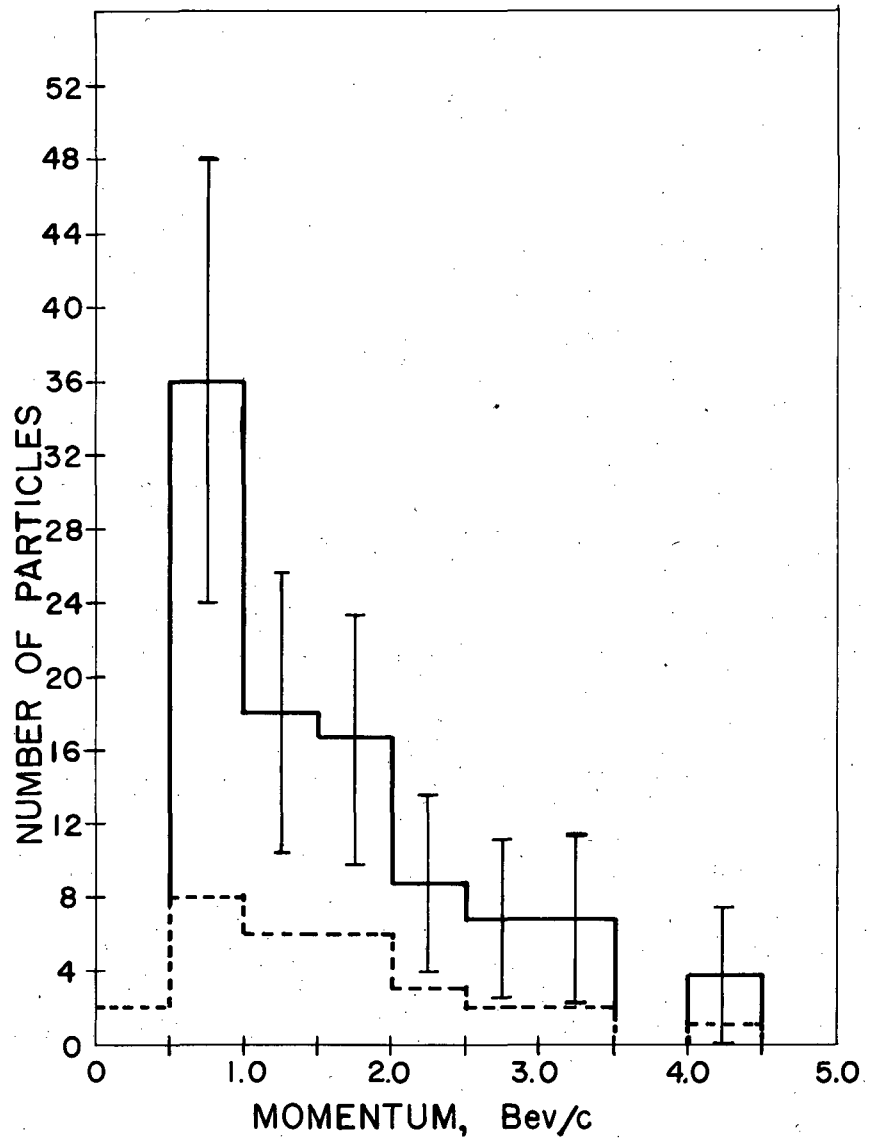
Fig. 20. Momentum distribution of neutron-produced $\wedge^0$'s. The dotted line is the actual number, the solid line is the weighted number of $\wedge^0$'s.
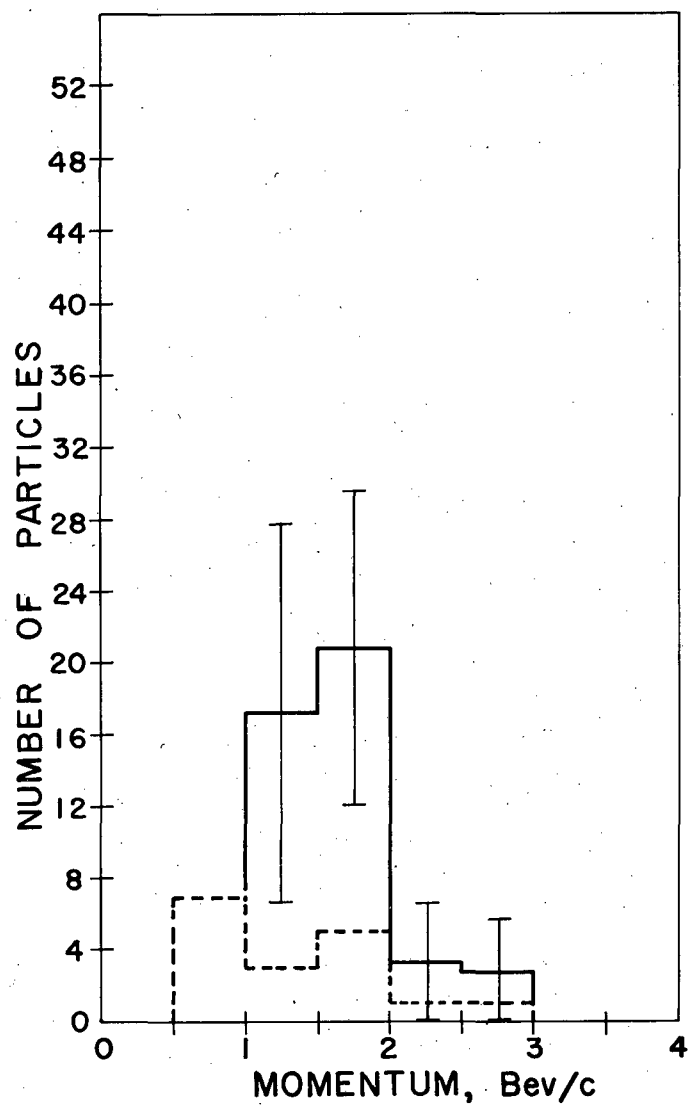
MU-11872

MU-11873

Fig. 21. Momentum distribution of neutron-produced θ^0's. The dotted line is the actual number, the solid line is the weighted number of θ^0's.

Ratios of Λ^0 Production to θ^0 Production

According to Gell-Mann and Pais, [10] the lowest-threshold allowed reactions that produce charged and neutral V particles in π^--nucleon collisions are

$$\pi^- + p \to \text{(i) } \Sigma^0 + \theta^0 \qquad\qquad (3\text{-a-i})$$

$$\text{(ii) } \Lambda^0 + \theta^0 \qquad\qquad (3\text{-a-ii})$$

$$\text{(iii) } \Sigma^- + K^+ , \qquad\qquad (3\text{-a-iii})$$

$$\pi^- + n \to \Sigma^- + \theta^0 ; \qquad\qquad (3\text{-b})$$

all other reactions require the emission of an additional particle. If one assumes that Reactions (3-a) and (3-b) dominate V^0 production, then since $\Sigma^0 \to \Lambda^0 + \gamma$ is a rapid decay, reactions (3-a) and (3-b) would imply equal numbers of Λ^0's and of θ^0's from π^- - p collisions, and θ^0's only from π^- - n. For π^- collisions with heavy nuclei, one would expect, therefore, a somewhat greater number of θ^0's produced than Λ^0's. In fact, if one assumes equal rates for all four reactions (3-a-i, ii, iii) and (3b) then the ratio of θ^0's produced to Λ^0's produced would be 1.5. Or, using the isotopic spin decomposition of states represented in Eqs. (3-a) and (3-b) into isotopic spin states 1/2 and 3/2, we find that the ratio of θ^0 to Λ^0 production would be $r = 2 \dfrac{(A3/2)^2}{(A_{1/2})^2}$, where $A_{3/2}$ and $A_{1/2}$ are the isotopic spin scattering amplitudes. The observed ratio for decays with momentum ≥ 1.0 Bev, after weighting for the detection efficiency of the chamber, is 1.73 ± 0.43, which is consistent with nearly equal isotopic spin amplitudes. The allowed reactions for nucleon-nucleon collisions, as given by the same authors, are

$$N + N \to \Lambda^0 + N + B , \qquad\qquad (4\text{-a})$$

$$N + N \to \Sigma + N + B , \qquad\qquad (4\text{-b})$$

where B is a heavy boson such as θ^0 or $\theta^\pm$. Enumerating the possibilities of (4-a), the lower-threshold reaction, we obtain

$$n + p \to \Lambda^0 + \theta^0 + p , \qquad\qquad (4\text{-a-i})$$

$$n + p \to \Lambda^0 + \theta^+ + n . \qquad\qquad (4\text{-a-ii})$$

$$n + n \rightarrow \Lambda^0 + \theta^0 + n, \qquad \text{(4-a-iii)}$$

$$p + p \rightarrow \Lambda^0 + \theta^+ + p. \qquad \text{(4-a-iv)}$$

If, owing to the lower threshold, these Reactions (4-a-i, ii, iii, iv) should dominate over those of (4-b), one would expect a greater fraction of Λ^0's to be produced in collisions of protons on nuclei than in collisions of neutrons on nuclei. From charge independence, A_0 and A_1 (amplitudes for scattering in the isotopic spin states 0 and 1, respectively) would both contribute to (4-a-i) and (4-a-ii) with the amplitude for (iii) and (iv) being A_1 only. For $A_0 = A_1$, the Λ^0/θ^0 ratio would be 3; it is > 1, for any choice. For neutron-nuclei collisions, one would still expect an excess of Λ^0's over θ^0's, but a smaller excess.

The observed ratios (after weighting for detection efficiency) are

$$\text{proton-nuclei } R_{p-Nu} = \frac{\text{number of } \Lambda^0}{\text{number of } \theta^0} = 2.1 \pm 2.1 \ ,$$

$$\text{neutron-nuclei } R_{n-Nu} = \frac{\text{number of } \Lambda^0}{\text{number of } \theta^0} = 1.36 \pm 0.55 \ .$$

This consistency with the above ideas, if not fortuitous within the large statistical error, may imply that at the energies used here reactions of the type (4-b) do not contribute substantially to V^0 production, or that similar relationships for these ratios continue to hold for the higher-threshold reactions.

Unfortunately the charged-V data, which could be very informative on these points, are not sufficiently definitive or statistically significant to aid in this analysis.

It is interesting to note the effect of adding an arbitrary number of $\pi^\pm$ and π^0 mesons to the right-hand side of Reactions (3) and (4), since these reactions without production of additional π mesons are rarely seen at these energies.[36]

In the nucleon-nucleon Reactions (4-a), where the ratio of Λ^0's to θ^0's should be greater than 1, this tendency should persist when additional π mesons are produced. The existence of charged θ's in this scheme, but no charged Λ's, allows the relative number of θ^0's to

diminish in favor of charged θ's, but the relative number of Λ^0's should stay the same. Thus the ratio of Λ^0's to θ^0's might stay the same or increase, but should not decrease. In the meson-nucleon Reactions (3), the presence of additional π mesons can influence the relative proportions of θ's as above, but also Λ^0's, since in these reactions some of the Λ^0's come from Σ^0 decay. However, because there are two reactions, (3-a-ii) and (3-b), in which Λ^0's (from Σ^0 decay) could now occur, as opposed to one (3-a-i) in which Λ^0's could cease to be produced (a charged Σ appearing instead of Σ^0), one might again expect the relative proportion of Λ^0 to θ^0 to increase. Thus the ratio obtained in this experiment,

$$R_{\pi-Nu} = \frac{\text{number of } \Lambda^0}{\text{number of } \theta^0} = 1/1.73 \cong 0.6 \ ,$$

might be still lower toward threshold.[37]

"Anomalous" Events

Among the measurable neutral V's found, there were four whose dynamics were clearly inconsistent with either the Λ^0 or θ^0 decay scheme. The pictures containing these events were checked carefully for unusual turbulence or photographic distortion. No evidence of either was found in these four pictures. In addition, the V^0's found in pictures closely preceding or following these were ascertained to be normal ones, as an additional check on the possibility of turbulence. One event originally thought anomalous was discovered in this way to be seriously affected by turbulence in the chamber gas. This event was then included with the normal V^0's after the measured uncertainties were increased according to the procedure for unusual turbulence described in the section on error (p. 15).

The dynamic characteristics of these "anomalous" decays are listed in Table IX of Appendix B.

In three of these four events, numbers 73456, 79497, and 81896, the ionization and momentum of the positive prong are such as to exclude a proton. The apparent two-body Q values, if both decay particles are assumed to be π mesons, are

$$\text{No. 73456, } Q\,(\pi\pi) = 96.0 \pm 8.5 \; ;$$

$$\text{No. 79497, } Q\,(\pi\pi) = 118.4 \pm 16.2 \; ;$$

$$\text{No. 81896, } Q\,(\pi\pi) = 101.9 + 7.6 \; .$$

These are consistent with a single-type two-body decay with $Q \sim 103$ Mev; but, more likely, are consistent with any of the following three-body decay schemes:[24,25,36]

$$\theta^0 \rightarrow \pi^{\pm} + \mu^{\mp} + \nu + 249 \text{ Mev} \;,$$

$$\rightarrow \pi^{\pm} + e^{\mp} + \nu + 354 \text{ Mev} \;,$$

$$\rightarrow \pi^{+} + \pi^{-} + \gamma + 214 \text{ Mev} \;.$$

It is unlikely that these are pairs from π^0 decays, since we have

$$\text{No. 73456, } Q(e^{+}e^{-}) = 468 \pm 5 \text{ Mev} \; ;$$

$$\text{No. 79497, } Q(e^{+}e^{-}) = 173 \pm 18 \text{ Mev} \; ;$$

No. 81896, Ionization rules out e^+,

and these Q values are greater than the rest mass of a π^0.

The remaining "anomalous" event, Number 75736, has an electron for the negative prong. The momentum and ionization of the positive prong indicate a mass greater than that of an L meson, but this is not certain. The following Q values were calculated:

$$Q(P^+ e^-) \cong 100 \pm 19 \text{ Mev },$$

$$Q(\pi^+ e^-) \cong 300 \pm 56 \text{ Mev },$$

making this decay consistent with

$$\Lambda^0 \rightarrow P^+ + e^- + \nu + 176.1 \text{ Mev },$$

$$\theta^0 \rightarrow \pi^+ + e^- + \nu + 354 \text{ Mev }.$$

Charged V Particles

Tables III and IV list the number of measurable charged-V decays obtained in the same series of experiments as the neutral V's. Those listed are limited to those decays that are consistent, within experimental error, with the two-body decay modes,

$$K^{\pm}_{\pi 2} \rightarrow \pi^{\pm} + \pi^0 + 203 \text{ Mev },$$

$$K^{\pm}_{\mu 2} \rightarrow \mu^{\pm} + \nu + 390 \text{ Mev },$$

$$\Sigma^{\pm} \rightarrow \pi^{\pm} + n + \sim 120 \text{ Mev },$$

$$\Sigma^+ \rightarrow p^+ + \pi^0 + \sim 116 \text{ Mev } .$$

In addition, Table V lists the charged decays that are inconsistent with the above modes, lumped with the unmeasurable cases.

All $V^{\pm}$ were selected according to the criterion $p \geq 300$ Mev/c for one of the tracks. Table IV lists those decay modes (out of the ones specified above) with which a given event is consistent within the experimental error. This classification was performed by use of the curves in Appendix A. The similarity of the dynamics of the charged decay modes, especially at high energies, relative to the experimental error of these measurements prevents the assignment of a unique mode (on the basis of dynamics) for most of the observed decays.

For this reason, reliable branching ratios of the various decay modes involving charged V's cannot be calculated. The tables exhibit only certain gross features of these branching ratios.

The average primary momentum of the V^- is 2.12 Bev/c; of the V^+, 2.25 Bev/c.

By assuming that the V^+ all have the lifetime of the θ^0, one can assign detection probabilities to each decay. Weighted numbers, correcting for those that decay outside the chamber, can then be calculated, as for the V^0's (see p. 24). Table VI lists the results in comparison to the neutral V's. The number of charged V's is small with a relatively large proportion of unidentified cases. It is consequently injudicious to attempt an interpretation in terms of the production reactions listed in the section "Ratios of Λ^0 Production to θ^0 Production," p. 49 .

Table III

Relative numbers of V particles produced by a given primary Bevatron beam. (Includes only those $V^{\pm}$ consistent with $K^{\pm}_{\pi 2}$, $K^{\pm}_{\mu 2}$, $\Sigma^{\pm}$ decay modes.)

| | Primary | | |
| | π^- | n | p |
Type V			
Λ^0	41	30	7
θ^0	39	17	4
V^+	3	4	1
V^-	10	6	1

Table IV

Number of charged V's consistent with a given decay mode for π^- and n Bevatron beams.

	Primary			
	V^+		V^-	
	π^-	n	π^-	n
Decay mode				
$K_{\pi 2}$	3	4	6	5
$K_{\mu 2}$	3	3	7	4
Σ	2	2	7	6

Table V

	Primary		
Type decay	π^-	$\underline{n}$	$\underline{p}$
V^+	4	5	4
V^-	2	2	0

Number of unidentified charged V's for each Bevatron beam.

Table VI

	Primary		
Type V	π^-	$\underline{n}$	$\underline{p}$
$\wedge^0$	93	60	12
θ^0	161	44	6
V^+	5	6	3

Relative weighted (for detection efficiency) numbers of V particles produced by given primary Bevatron beams. Includes only those V's having momentum ≥ 1.0 Bev/c.

Associated Production

The detection efficiency (Fig. 8) for observing a θ^0 and a Λ^0 of roughly the same momentum in the region 1.0 to 3.0 Bev/c averages about 0.06. Since both the θ^0 and Λ^0 laboratory-system angular distributions (Figs. 10A and 10B) are sharply peaked forward, one would not expect to lose a large percentage of one of a pair simultaneously produced, because of the chamber geometry. Towards the edge of the sensitive region one would expect to lose up to 50% of an angular distribution into the region outside the sensitive volume if the beam area were sharply defined. If this percentage is a lower limit, then, the combined detection efficiency at the lower limit is 0.03. If a second V^0 is consistently produced with the observed one and decays in an observable mode, then since 124 V^0's were found in the 1.0-to 3.0-Bev/c region, four or more pictures with two V^0's should have been found. Since, in fact, no pictures were found with more than one wall-produced V^0, this supports the hypothesis of invisible decay modes if associated production is the rule. However, because of the lower detection efficiency in this experiment, this evidence is not as strong as that found by Blumenfeld, Booth, Lederman, and Chinowsky,[35] and by other experimenters. Since the actual production point in the wall is not determinable for the V^0's in this experiment, it is not feasible to calculate a line of flight by assuming the process $\pi^- + p \rightarrow \Lambda^0 + \theta^0$, and then search for the unobserved V^0. Further, at these energies, no examples of the above process without the production of additional particles have been observed.[17]

ACKNOWLEDGMENTS

APPENDICES

A. Formulae and Graphs

List of Formulae (Quantities undefined here are defined in Appendix B)

1. Angle between production and decay planes, ϕ:

$$\cos \phi = \frac{1}{\sin \theta \, \sin \alpha'} \times \left\{ \cos \alpha_0 \left[\cos \alpha_1 \, \sin \alpha_2 \, \cos \beta_2 - \cos \alpha_2 \, \sin \alpha_1 \, \cos \beta_1 \right] \right.$$

$$\left. - \sin (\beta_2 - \beta_1) \, \sin \alpha_0 \, \sin \beta_0 \, \sin \alpha_1 \, \sin \alpha_2 \right\} \, ,$$

where $\cos \alpha_0 = \dfrac{P_z}{P}$, $\sin \alpha_0 \, \sin \beta_0 = \dfrac{P_y}{P}$,

$$\sin \alpha_0 \, \cos \beta_0 = \frac{P_x}{P} = \cos \alpha' \, .$$

2. Angle between decay plane and magnetic field $\vec{B}$ (direction of $\vec{B}$ is $\alpha = 0$):

$$\cos \eta = \frac{\sin \alpha_1 \, \sin \alpha_2 \, \sin (\beta_2 - \beta_1)}{\sin \theta} \, .$$

3. Emission angle relative to line of flight in proper system of V^0:

$$\sin \theta_{CMS} = \frac{P_1 P_2 \, \sin \theta}{p \, p^*} \, ,$$

where $p^* = $ center-of-mass momentum.

4. Angle of $\vec{p_1}$ with respect to the normal to the production plane:

$$\cos y = \frac{P_2}{p \sin \alpha'} \, (\sin \alpha_1 \, \sin \beta_1 \, \cos \alpha_2 - \sin \alpha_2 \, \sin \beta_2 \, \cos \alpha_1) \, .$$

5. Angle of production-plane normal with respect to the vertical:

$$\cos \chi = \frac{-P_y}{p \sin \alpha'} \, .$$

6. Derivatives:[13]

$$\frac{\partial Q}{\partial P_+} = \frac{E - P_+}{E_+} - P - \cos\theta / M_+ + M_- + Q \, ,$$

$$\frac{\partial Q}{\partial P_-} = \frac{E_+ \, P_-}{E_-} - P_+ \, \cos \theta / M_+ + M_- + Q \, ,$$

$$\frac{\partial Q}{\partial \theta} = \frac{P_+ \, P_- \, \sin \theta}{(M_+ + M_- + Q)} \, ,$$

$$E \equiv \text{total energies}.$$

Graphs

The following graphs, Figs. 22-37, represent the equation

$$E_1 E_2 - p_1 p_2 \cos \theta = \text{constant},$$

which holds for both neutral and charged V's if θ is interpreted as the opening angle for neutral V's and the deflection angle for charged V's.

The dotted line on Fig. 25 distinguishes between forward and backward protons for Λ^0 decay. Those Λ^0's falling on the right side of the line have forward protons in the center of mass of the decay, and those falling on the left have backward protons.
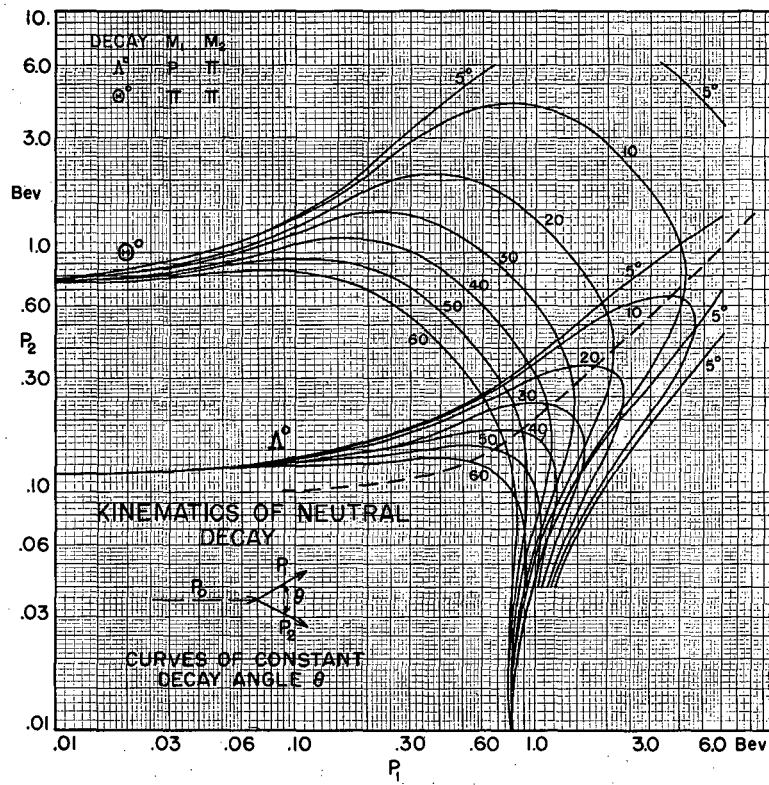
Fig. 22
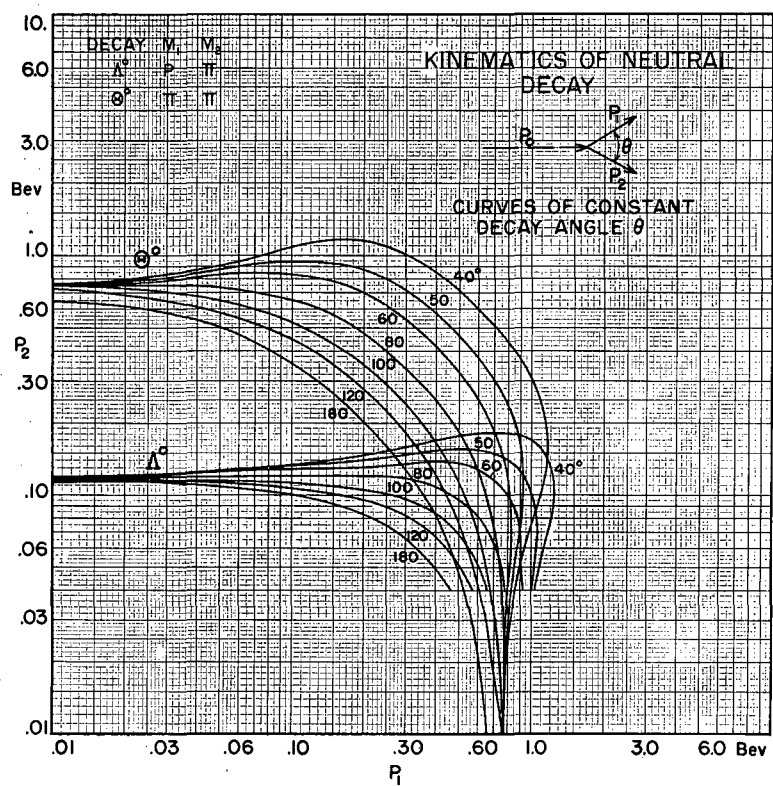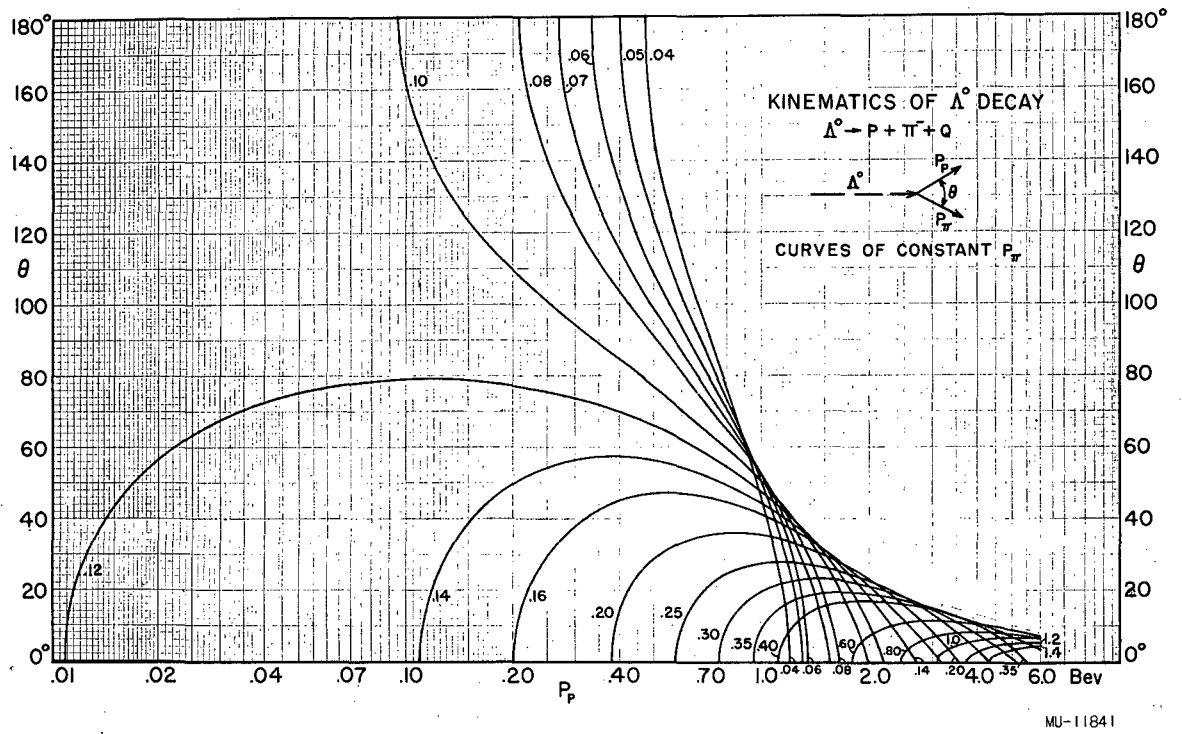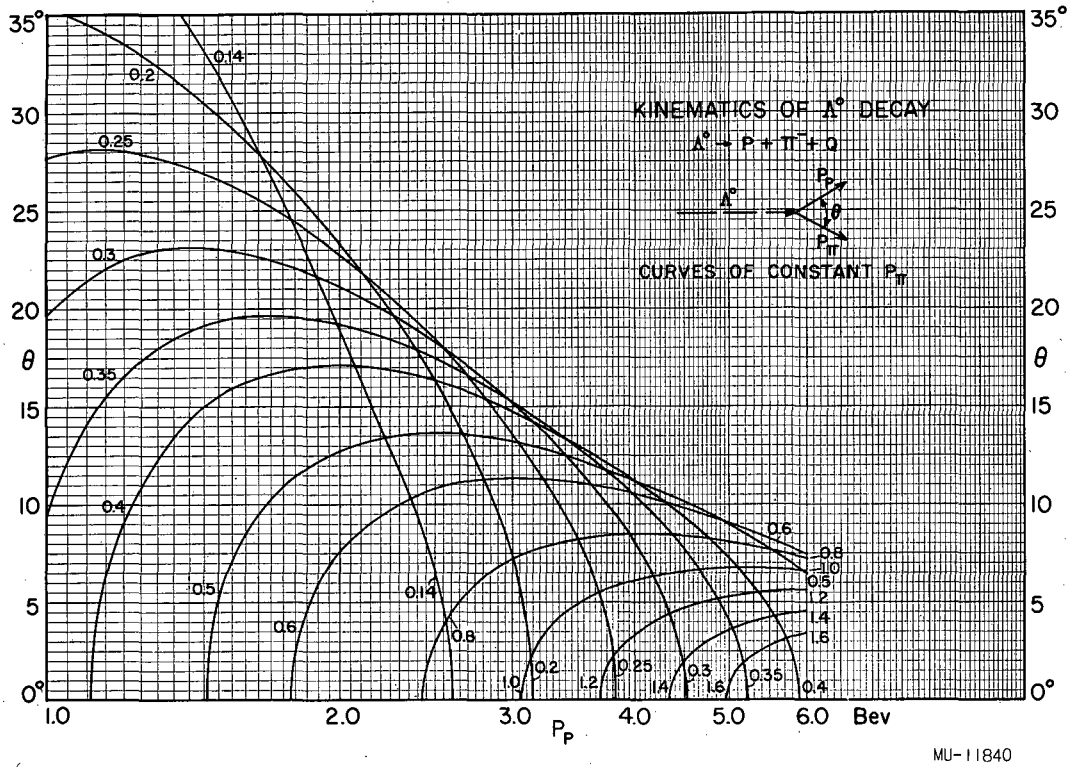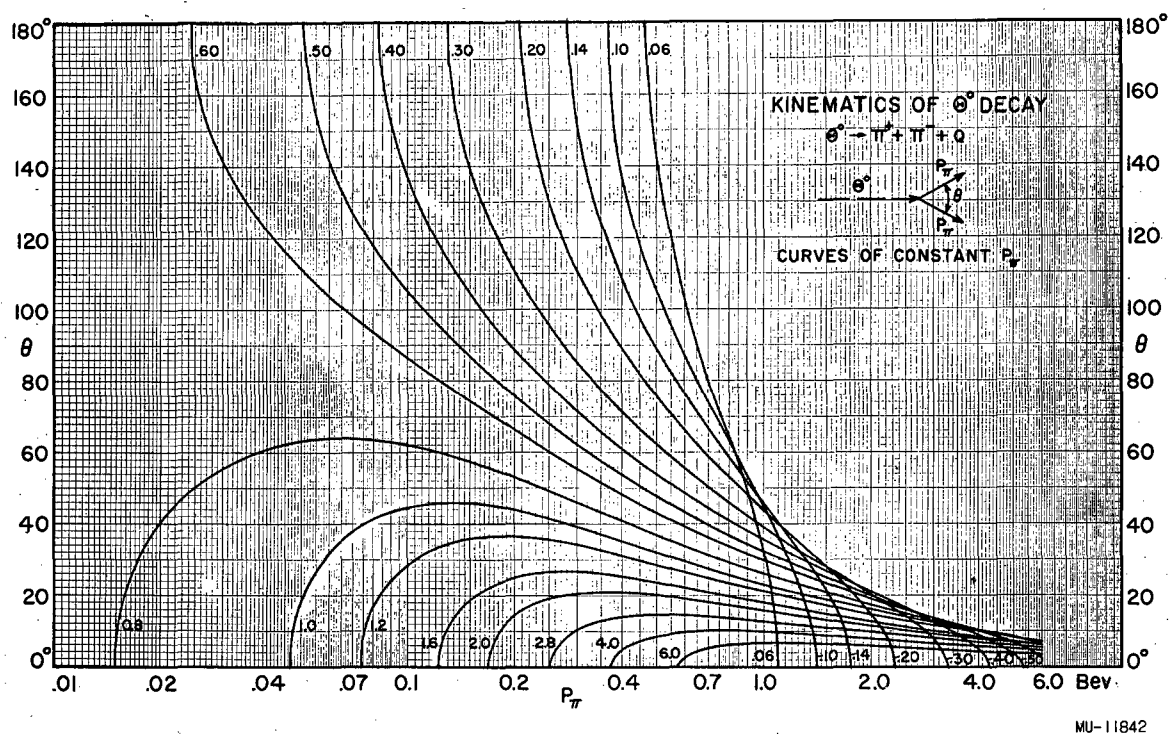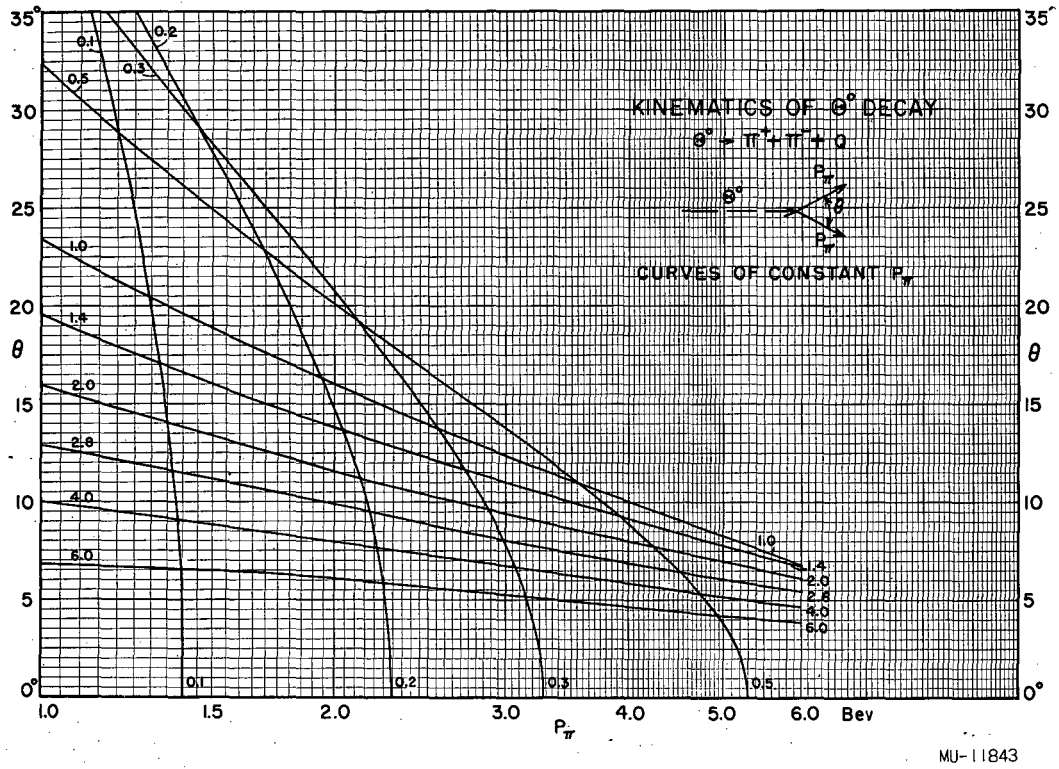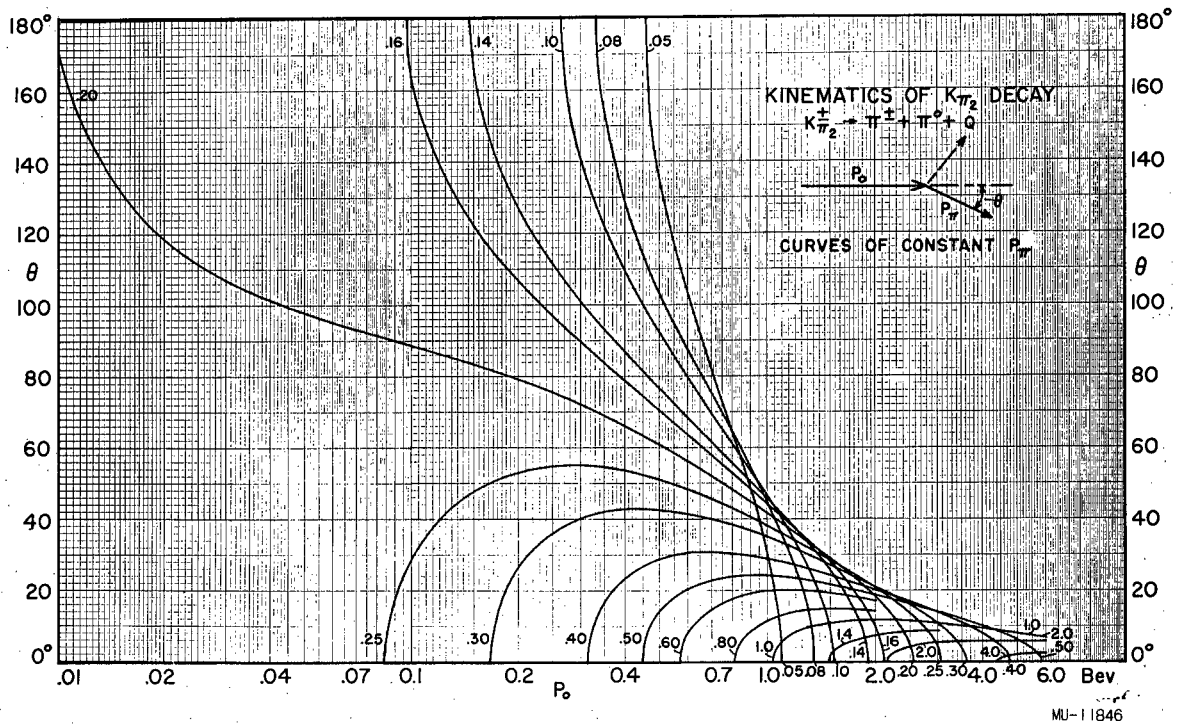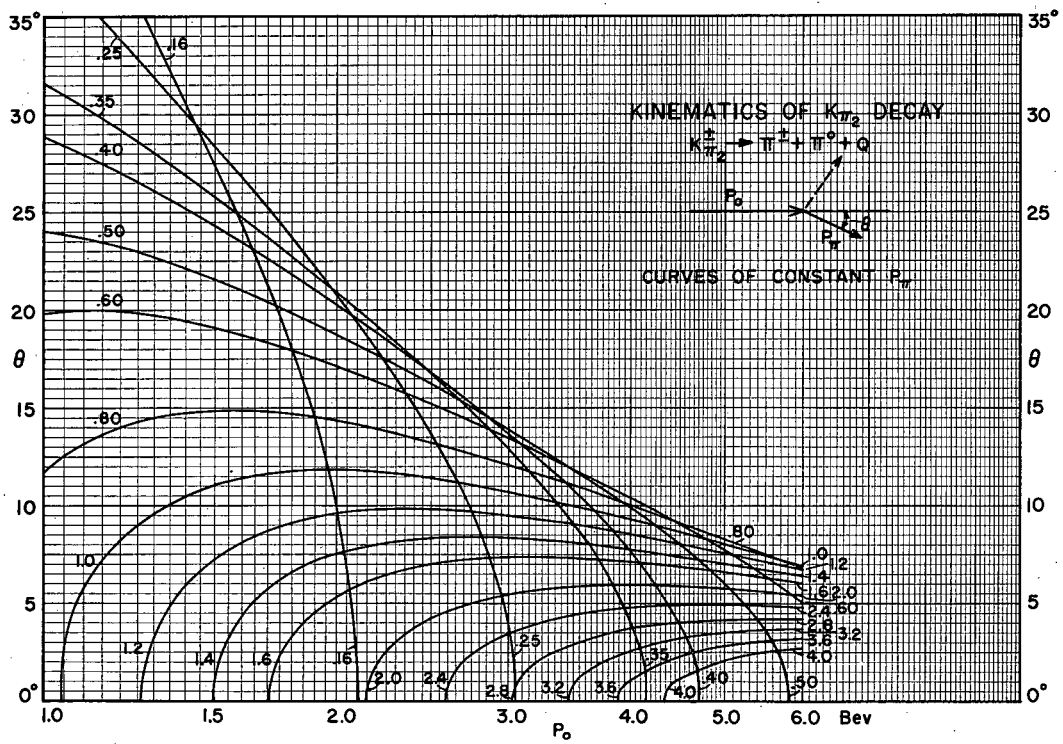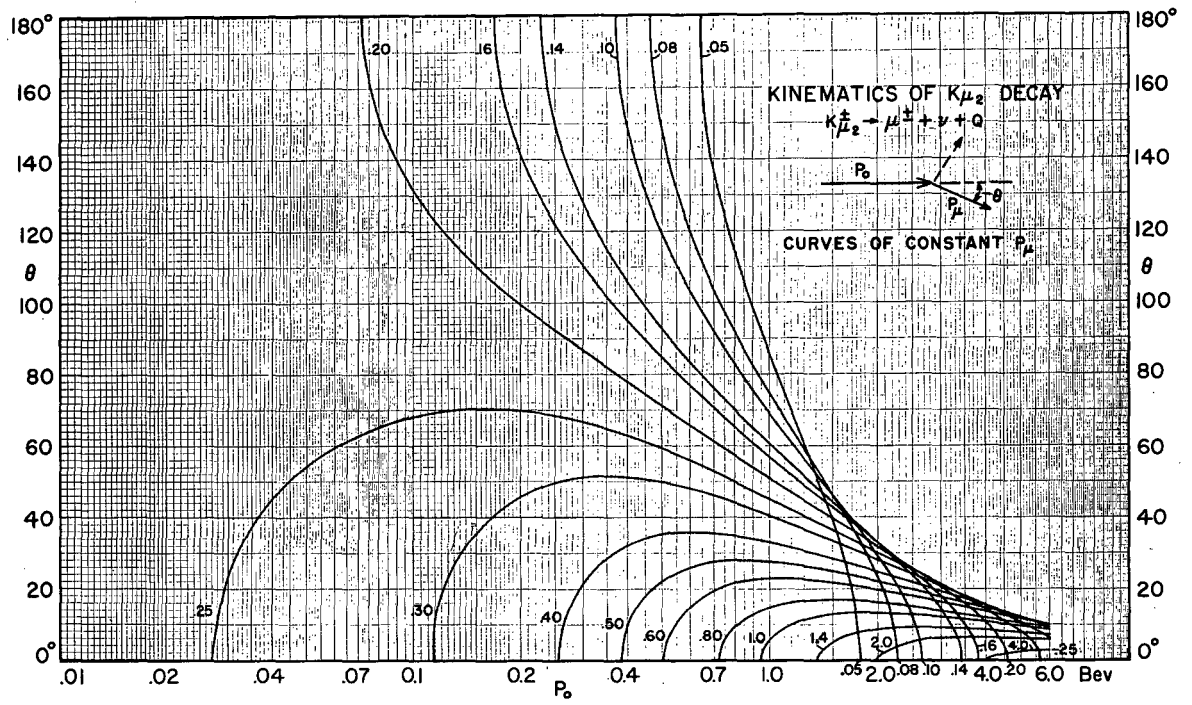
Fig. 23

MU-11845

KINEMATICS OF Λ° DECAY

Λ° → P + π⁻ + Q

CURVES OF CONSTANT P_π

Fig. 24

Fig. 25

Fig. 26

Fig. 27

Fig. 28

Fig. 29

KINEMATICS OF $K\mu_2$ DECAY

$K^{\pm}_{\mu_2} \rightarrow \mu^{\pm} + \nu + Q$

CURVES OF CONSTANT P_μ

Fig. 30

MU-11848

-70-

Fig. 31

Fig. 32

KINEMATICS OF $\Sigma^{\pm}$ DECAY
$\Sigma^{\pm} \rightarrow n + \pi^{\pm} + 0$

CURVES OF CONSTANT P_π

MU-11854

Fig. 33

Fig. 34

Fig. 35

MU-11853

- 75 -

KINEMATICS OF Ξ DECAY

Ξ → Λ° + π + Q

CURVES OF CONSTANT Pπ

MU-11849

Fig. 36

KINEMATICS OF Ξ DECAY

$\Xi \rightarrow \Lambda^0 + \pi + Q$

CURVES OF CONSTANT P_π
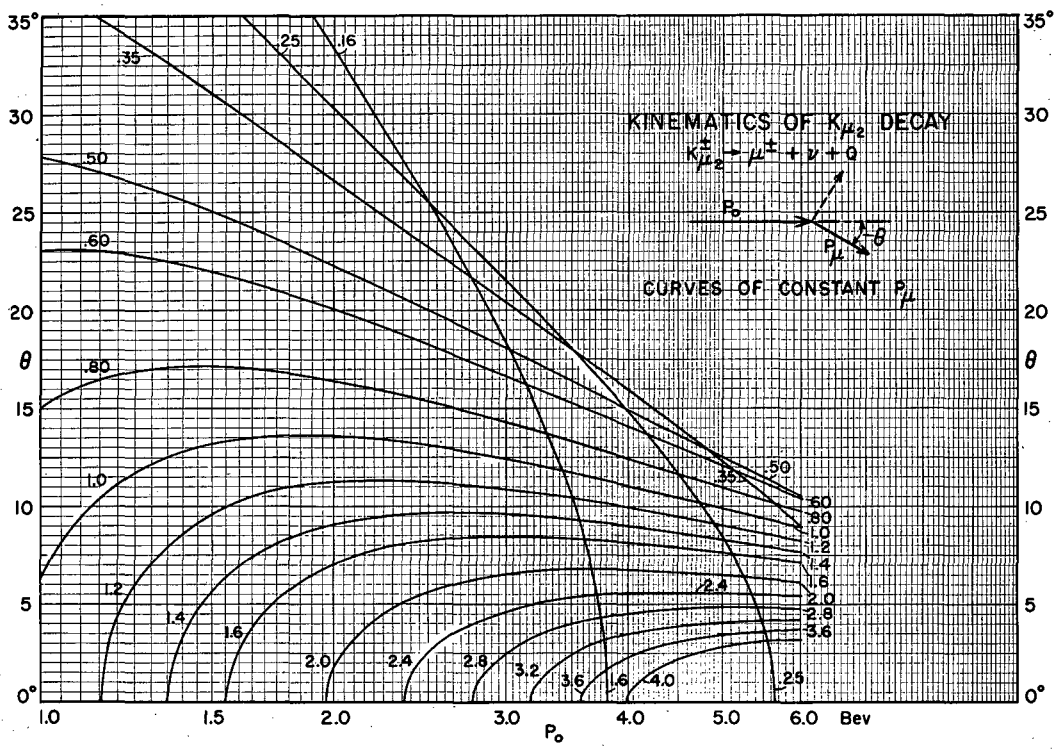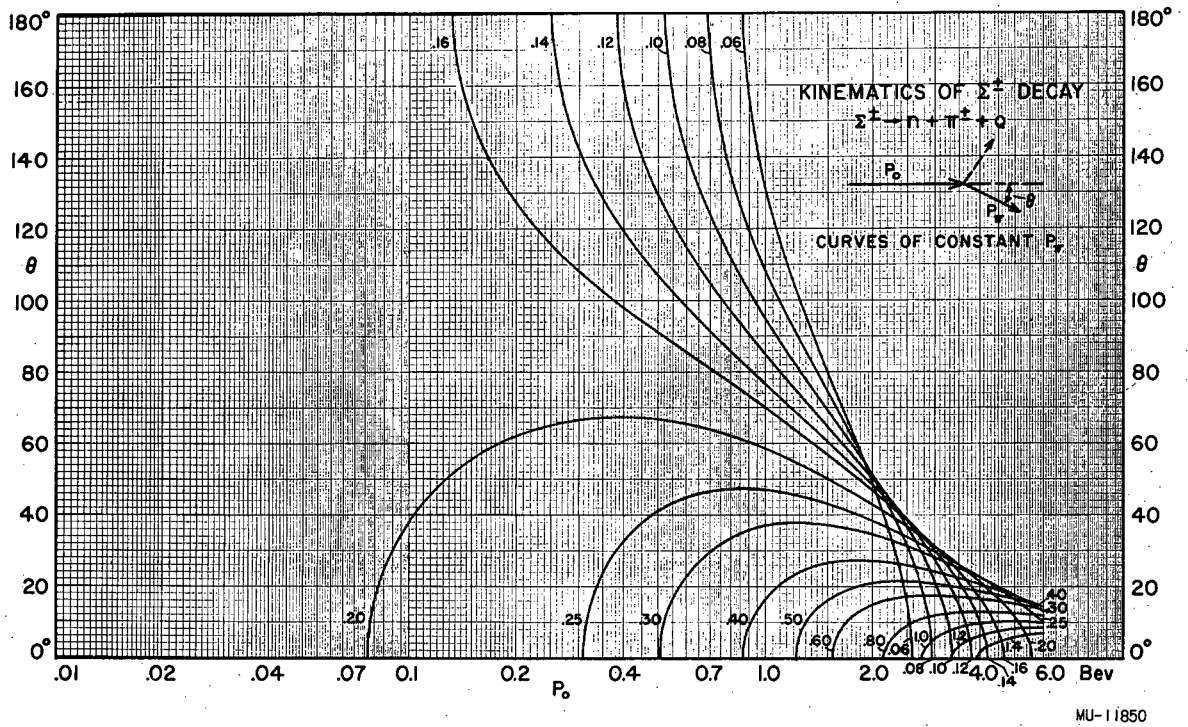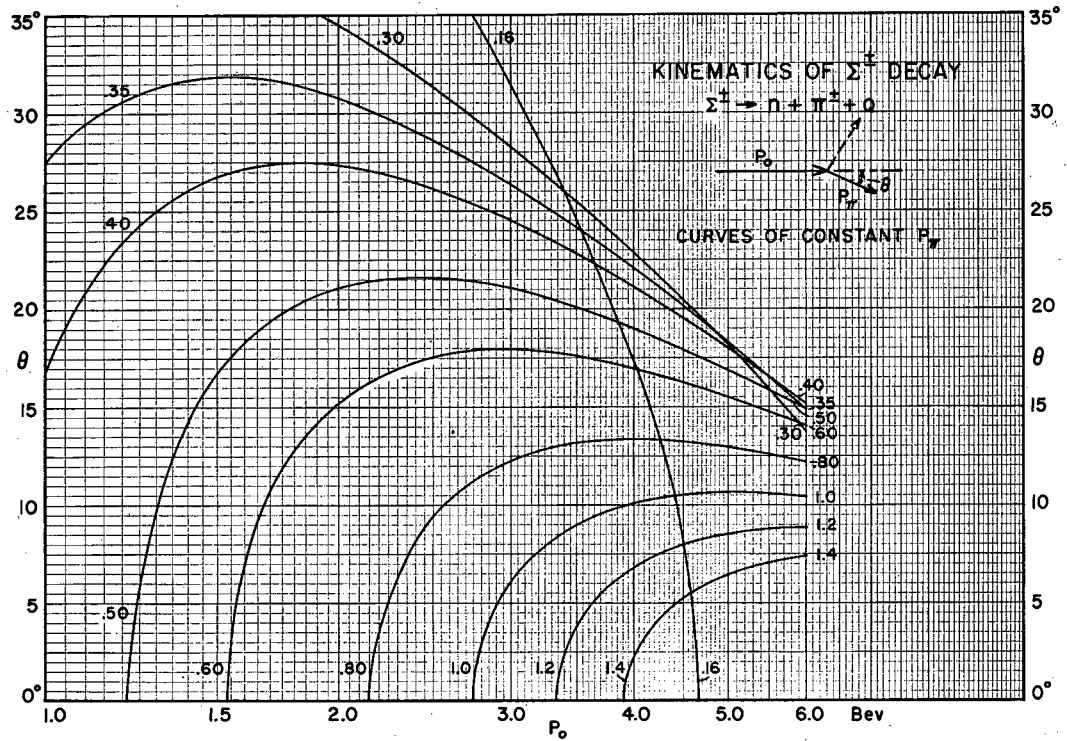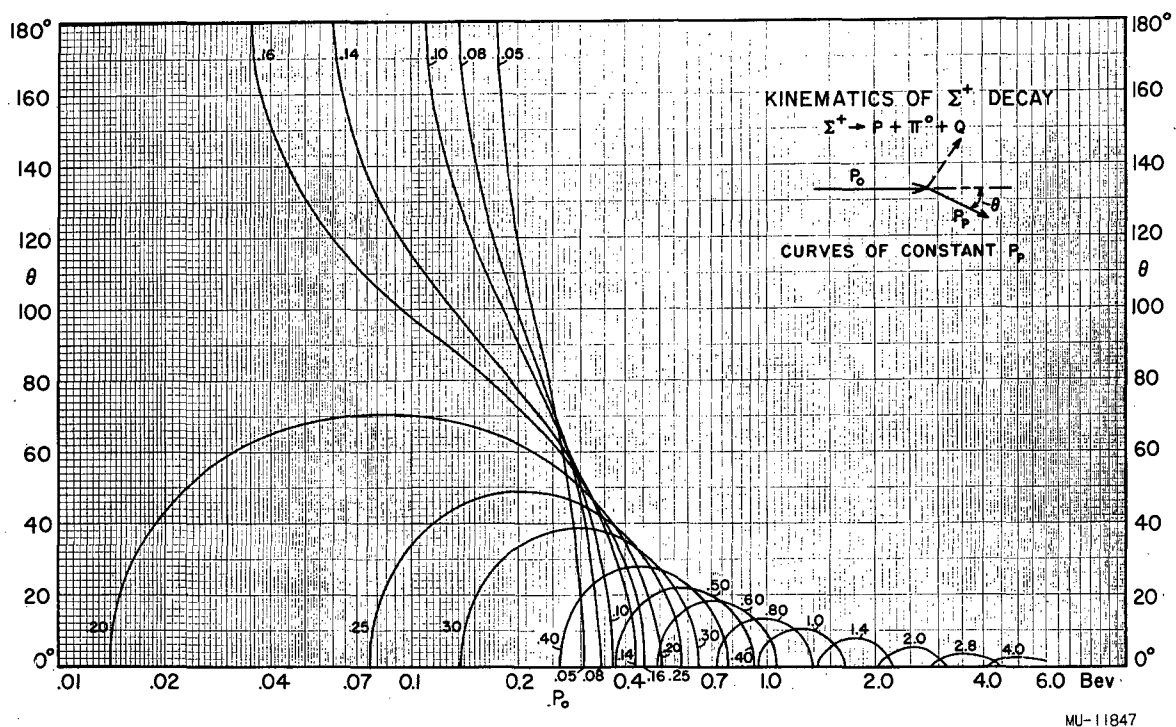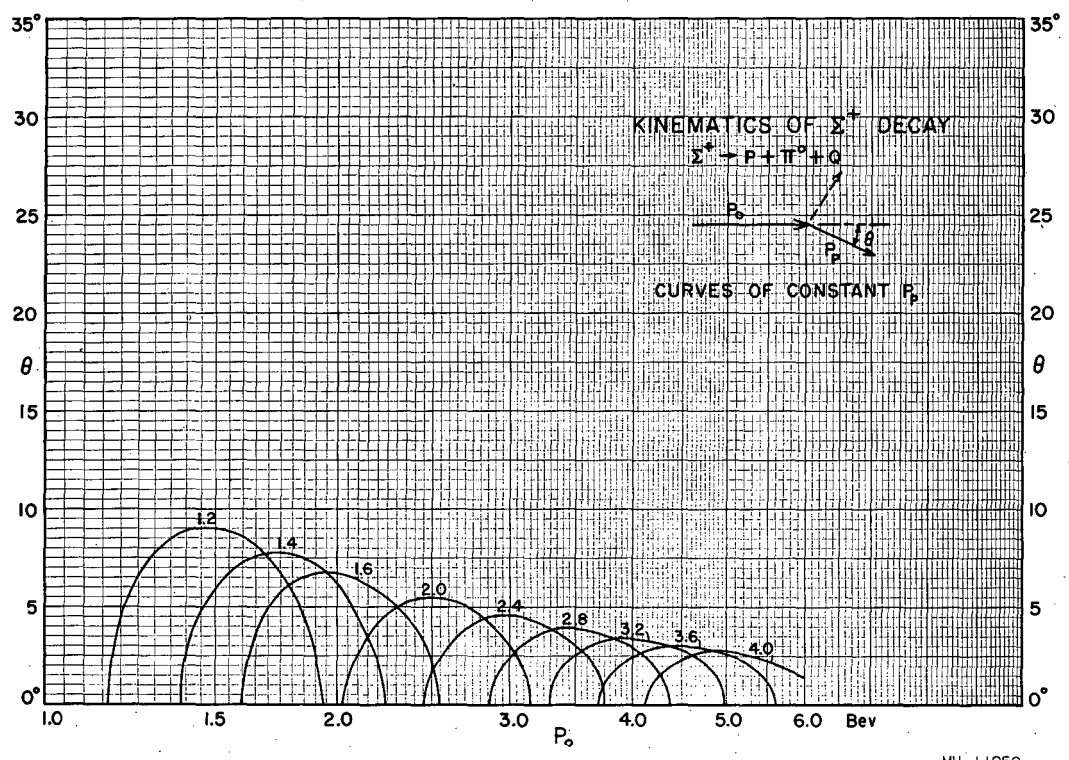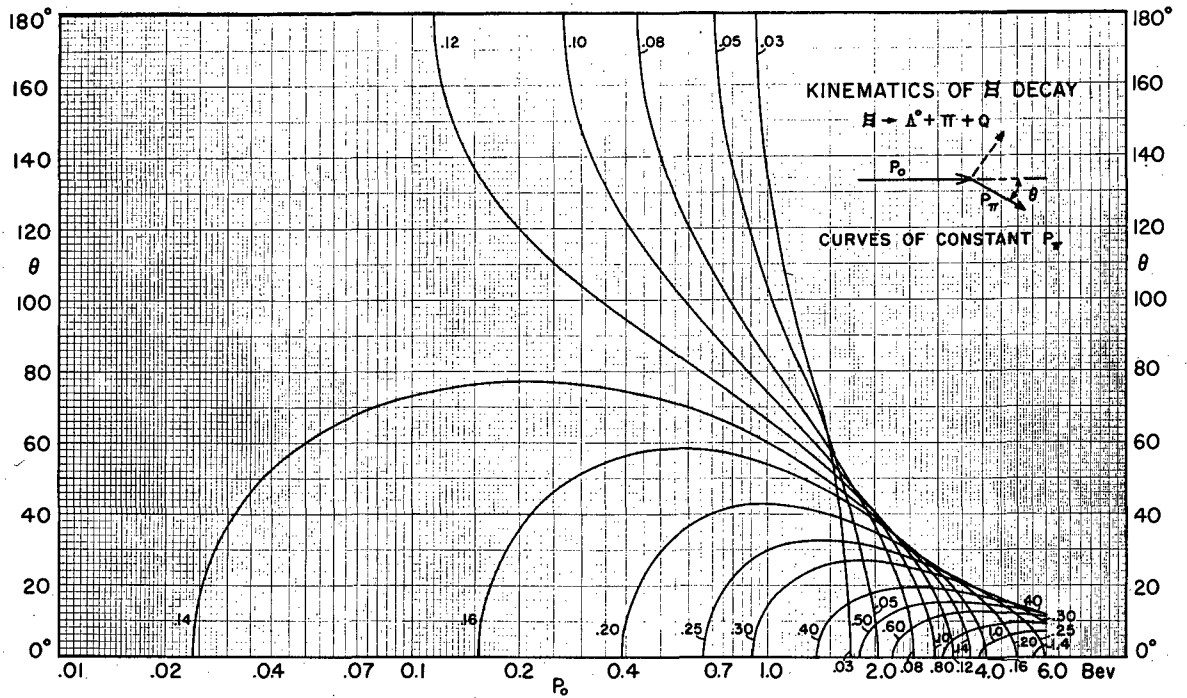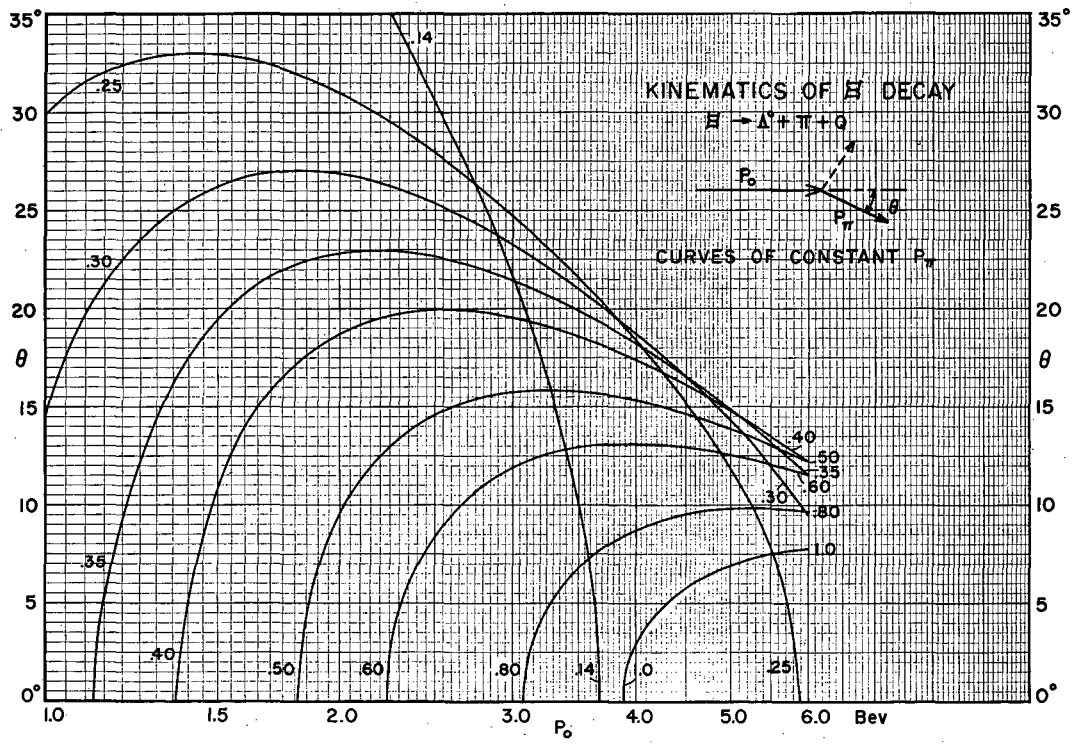
Fig. 37

MU-11855

B. Catalogue of Decay Events Observed in 36-Atmosphere Chamber

The quantities listed at the column heads in the tables that follow are defined as:

p_+ = momentum of positive prong in Bev/c.

p_- = momentum of negative prong in Bev/c.

θ = opening angle between prongs for neutral V's and deflection angle between prongs for charged V's.

$p = \sqrt{p_+^2 + p_-^2 + 2p_+ \, p_- \cos \theta}$ = total momentum vector of V in Bev/c.

ϕ = angle between production plane and decay plane.

η = angle between decay-plane normal and magnetic field.

χ = angle between production-plane normal and magnetic field.

α' = polar angle of total momentum vector $\vec{p}$ with respect to the incoming beam.

$\left[\dfrac{(dE)}{(dx)}\right]_\pm$ = ionization relative to minimum for + and - prongs, respectively. M, signifying minimum, is inserted in this column where the momentum is sufficiently high to render a numerical estimate by eye superfluous.

$W = \dfrac{1}{P(p)}$ = weight assigned each decay, P(p) being the detection probability for a V^0 of momentum p. This weight is equal to the number of V^0's that pass through the chamber at a given momentum for each one observed to decay.

Q = energy release in decay, assuming (p^+, π^-) decay mode for Λ^0, (π^+, π^-) for θ^0.

Nominal errors of measurement values on these variables are as follows:

θ	$\pm 1.0^\circ$
η	$\pm 0.6^\circ$
$Q(\Lambda^0)$	± 8 Mev
$Q(\theta^0)$	± 40 Mev
p	$\pm 10\%$
ϕ	$\pm 6^\circ$
α'	$\pm 0.9^\circ$
χ	$\pm 0.8^\circ$

Table VII. Λ^0

π^- Production

Film#	p_+	p_-	$\left(\dfrac{dE}{dx}\right)_+$	$\left(\dfrac{dE}{dx}\right)_-$	θ	p	ϕ	η	χ	$\cos \alpha'$	W	Q
51823	1.7182	0.3850	M	M	18.5°	2.088	160.0	23.5	180.0	0.9914	2.81	36.9
53861	2.0587	0.6427	M	M	7.3	2.698	88.5	159.3	79.3	0.9999	2.95	39.3
55206	1.1662	0.4056	1.0-1.7	1.0-1.3	10.5	1.567	115.8	119.9	124.4	0.9949	2.79	41.8
55265	1.3748	0.3958	1.0-1.2	1.0-1.1	13.0	1.762	43.1	22.3	61.0	0.9541	2.78	34.6
56566	0.5837	0.1895	2.0-4.0	1.0-1.3	35.2	0.748	31.7	66.7	94.8	0.9155	4.20	34.8
56629	0.8570	0.1735	1.1-1.6	1.0-1.4	44.6	0.988	175.3	167.8	16.3	0.7607	3.31	41.9
56882	2.4256	0.9694	M	M	6.7	3.390	153.4	37.9	168.8	0.9918	3.29	72.3
58061	1.7559	0.5633	M	M	4.5	2.318	76.8	120.0	52.0	0.9792	2.87	34.1
59063	0.8815	0.3212	1.1-1.5	1.0-1.1	12.3	1.198	146.3	22.3	131.5	0.8015	2.99	39.2
59064	2.6512	0.6098	M	M	9.7	3.254	102.3	164.9	70.8	0.9853	3.22	32.5
59435	0.9380	0.3497	1.1-1.2	1.0-1.1	9.0	1.284	97.4	103.8	5.8	0.9688	2.92	40.7
60052	1.9862	0.5400	1.0-1.4	1.0-1.1	13.0	2.515	156.4	140.7	71.6	0.9984	2.93	44.7
60304	1.4595	0.3452	1.0-1.2	1.0-1.1	20.5	1.814	138.4	17.5	155.9	0.9994	2.78	38.9
62310	0.5746	0.2497	1.4-3.0	1.0-1.1	13.3	0.820	43.2	139.9	106.5	0.9603	3.85	40.0
62317	1.4368	0.1564	1.0-1.5	1.0-1.5	34.7	1.568	16.7	38.5	21.9	0.9974	2.79	39.7
63522	1.0230	0.2500	1.0-1.3	1.0-1.7	29.0	1.247	115.7	31.6	14.6	0.9955	2.94	39.1
66658	1.6059	0.1775	1.0-1.5	1.0-1.7	29.7	1.762	71.4	122.5	165.9	0.9784	2.78	37.8
67727	0.9203	0.2067	1.1-1.3	1.1-1.2	36.6	1.093	85.5	9.6	87.5	0.9823	3.12	40.2
67737	0.9840	0.3555	1.1-1.6	1.0-1.1	15.4	1.330	165.2	19.9	175.6	0.9569	2.90	46.3
67898	0.5571	0.2182	1.3-2.5	1.0-1.3	29.8	0.755	16.3	154.1	171.9	0.9441	4.22	41.9
68923	0.6319	0.2438	2.0-4.0	1.5-2.0	22.3	0.862	29.3	34.2	5.1	0.9240	3.68	40.3

$$\Lambda^0$$

Film#	p_+	p_-	$\left(\dfrac{dE}{dx}\right)_+$	$\left(\dfrac{dE}{dx}\right)_-$	θ	p	ϕ	η	χ	$\cos a'$	W	Ω
69091	0.9878	0.3714	1.0-1.5	1.0-1.3	11.7	1.354	93.0	96.9	2.5	0.9454	2.87	45.6
69833	0.8400	0.2432	1.1-1.5	1.0-1.5	30.9	1.057	42.3	12.8	33.7	0.9550	3.17	42.0
69919	1.7233	0.5347	1.1-1.3	1.0-1.1	9.2	2.252	48.3	134.8	176.9	0.9683	2.86	41.6
79827	0.8306	0.1150	1.2-3.0	1.2-3.5	56.9	0.898	119.6	84.0	156.1	0.9957	3.53	39.7
80617	1.2539	0.2578	1.1-1.5	1.0-1.5	28.5	1.485	137.3	26.1	160.2	0.9952	2.83	40.2
80628	1.2249	0.4650	1.0-1.3	1.0-1.2	3.9	1.689	63.4	82.7	145.9	0.9952	2.78	45.3
80713	0.6419	0.1553	1.3-1.8	1.1-1.5	51.9	0.748	35.3	153.1	163.6	0.6754	4.22	40.8
80794	0.5021	0.1453	1.5-3.5	1.1-2.0	59.0	0.591	27.5	34.7	61.5	0.9859	5.71	41.2
81232	2.1965	0.5216	M	M	12.6	2.708	1.7	157.8	164.6	0.9802	3.01	35.9
81432	1.0600	0.3460	1.0-1.3	1.0-1.1	11.1	1.401	22.7	29.1	5.8	0.9542	3.86	34.0
81812	1.3657	0.4481	1.0-1.5	1.0-1.3	10.1	1.809	102.5	116.9	133.5	0.9879	2.78	40.3
82351	1.4441	0.3969	1.2-1.6	1.1-1.4	11.2	1.835	76.7	17.6	73.9	0.9932	2.78	27.9
82422	1.3277	0.2554	1.0-1.5	1.0-1.2	29.0	1.556	73.0	62.8	109.3	0.9959	2.79	41.2
82602	1.2338	0.0747	1.2-2.5	2.0-4.0	40.4	1.292	58.5	97.3	25.4	0.9790	2.92	40.3
84107	0.8443	0.2844	1.1-1.6	1.0-1.1	21.7	1.112	12.2	28.0	38.6	0.9802	3.08	41.8
84876	0.9231	0.2542	1.0-2.0	1.0-1.5	2.19	1.163	76.5	114.2	42.7	0.8450	3.03	30.2

$$\Lambda^0$$
Neutron Production

Film#	p_+	p_-	$\left(\dfrac{dE}{dx}\right)_+$	$\left(\dfrac{dE}{dx}\right)_-$	θ	p	ϕ	η	χ	$\cos a'$	W	Q
71223	0.9882	0.0944	1.2-2.5	1.5-5.0	42.2	1.060	17.2	4.5	18.2	0.9784	3.8	26.8
71639	1.5002	0.6520	M	M	9.0	2.146	166.5	164.2	9.8	0.9466	2.83	75.7
72061	1.7928	0.6157	M	M	12.0	2.399	111.0	101.4	8.9	0.9790	2.90	59.4
73008	0.7464	0.1302	1.3-1.8	1.1-1.5	68.4	0.807	19.3	124.9	144.1	0.9524	3.89	53.6
73219	0.6319	0.2121	1.1-2.0	1.0-1.3	29.4	0.823	3.0	161.3	158.6	0.9519	3.83	36.1
73262	0.7531	0.0570	1.1-1.6	2.5-4.0	68.0	0.776	146.9	152.2	2.6	0.9829	4.08	31.5
73577	0.6361	0.0866	1.4-2.5	1.5-3.0	73.0	0.667	4.9	51.1	55.7	0.9895	4.83	35.8
73580	2.8110	0.6659	1.0-1.6	1.0-1.7	9.6	3.469	123.2	120.5	9.1	0.9955	3.23	37.2
73718	1.4821	0.4137	1.0-1.2	1.0-1.2	13.1	1.885	157.9	180.0	15.4	0.9845	2.78	39.2
74728	1.2760	0.2929	1.1-1.4	1.0-1.1	31.3	1.533	143.4	66.7	104.8	0.9504	2.79	58.2
74773	0.5950	0.0951	1.5-2.5	1.2-1.5	77.9	0.622	61.2	11.8	86.5	0.9845	5.26	40.8
74792	1.2791	0.4084	1.1-1.5	1.0-1.1	15.6	1.676	81.6	71.2	16.7	0.8653	2.78	45.7
74795	0.8665	0.3446	1.0-1.5	1.0-1.1	21.0	1.194	52.0	116.2	166.4	0.8936	2.99	59.2
74808	2.7612	0.6978	1.0-1.5	1.0-1.5	7.8	3.454	25.9	5.1	20.5	0.9973	3.32	32.7
75177	0.5619	0.1495	1.1-1.6	1.1-1.6	50.7	0.667	69.8	78.0	145.8	0.9324	4.83	36.2
75532	1.2545	0.0531	1.0-2.0	2.0-5.0	26.0	1.303	24.8	152.1	180.0	0.9668	2.90	39.0
75597	1.8800	0.4786	1.0-1.2	1.0-1.2	11.7	2.349	126.7	119.2	113.4	0.9933	2.87	36.8
75651	0.6244	0.2407	1.5-4.0	1.0-1.1	30.7	0.840	60.6	64.3	4.5	0.9609	3.73	48.6
77534	1.3486	0.4606	1.0-1.2	1.0-1.1	11.0	1.803	114.0	167.7	64.5	0.9910	2.78	45.3
77564	0.4190	0.1958	3.0-5.0	1.0-1.3	29.0	0.598	131.0	127.3	14.8	0.9444	5.56	40.4
77642	1.9828	0.6086	M	M	7.1	2.587	12.8	86.8	74.2	0.9894	2.95	37.5

$$\Lambda^0$$

Film #	p_+	p_-	$\left(\dfrac{dE}{dx}\right)_+$	$\left(\dfrac{dE}{dx}\right)_-$	θ	p	ϕ	η	χ	$\cos \alpha'$	W	Q
78176	2.0376	0.5008	M	M	12.5	2.529	104.7	172.3	75.9	0.9767	2.94	36.4
78634	1.2390	0.3241	1.3-1.7	1.1-1.3	21.0	1.546	58.4	67.1	24.7	0.9856	2.79	38.6
78707	0.3043	0.1675	2.0-3.0	1.0-1.5	33.9	0.426	161.3	24.1	116.2	0.7498	-	48.8
79686	1.3325	0.3826	1.0-1.3	1.0-2.0	13.5	1.707	123.5	110.7	122.1	0.9951	2.78	34.4

$$\wedge^0$$

Proton Production

Film#	p_+	p'_-	$\left(\dfrac{dE}{dx}\right)_+$	$\left(\dfrac{dE}{dx}\right)_-$	θ	p	ϕ	η	χ	$\cos a'$	W	Q
87106	1.8748	0.4444	M	M	16.1	2.306	109.6	70.6	38.6	0.9920	2.87	39.9
87223	0.6457	0.2209	1.5-4.0	1.1-1.3	24.8	0.852	88.3	82.0	170.1	0.9224	3.70	33.8
88020	1.9947	0.6219	M	M	12.7	2.980	176.3	145.0	8.5	0.9609	3.11	45.0
88830	0.9360	0.2279	1.1-2.0	1.0-2.0	33.1	1.137	51.1	50.4	99.1	0.8819	3.04	40.5
89198	0.6276	0.1670	1.8-4.0	1.0-1.5	57.7	0.732	78.9	79.9	146.7	0.9849	4.35	52.2

Table VIII. θ^0

π^- Production

Film#	p_+	p'_-	$\frac{dE}{dx}_+$	$\frac{dE}{dx}_-$	θ	p	ϕ	η	χ	$\cos \alpha'$	W	Q
51836	0.9151	0.5254	M	M	32.1	1.389	106.1	61.6	169.6	0.9889	5.18	200.9
58583	0.0990	1.2182	2.5-5.0	1.0-1.1	37.1	1.298	6.4	65.5	19.9	0.9996	5.74	237.1
58846	0.9960	0.4234	M	M	34.9	1.367	1.2	94.8	174.9	0.8832	5.26	209.1
60614	0.6021	0.6263	M	M	43.3	1.138	159.1	110.5	27.0	0.9861	7.14	257.5
61633	1.3052	0.9117	M	M	22.5	2.173	58.5	123.7	180.0	0.9116	3.28	243.1
62131	1.2636	0.5593	M	M	29.2	1.774	69.8	109.7	37.8	0.9929	3.89	238.8
62991	1.0112	1.5830	M	M	20.4	2.555	50.9	126.6	168.3	0.999	3.01	252.3
67277	1.5736	1.3657	M	M	19.1	2.900	152.0	30.4	92.6	0.913	2.88	274.9
67349	1.1118	0.8374	M	M	23.2	1.917	79.5	78.9	158.1	0.9876	3.60	170.1
67460	0.4286	1.5395	1.0-1.1	1.0-1.1	22.3	1.943	175.3	6.8	171.5	0.9970	3.57	180.3
68239	2.5961	0.8863	M	M	12.0	3.470	45.3	146.4	105.1	0.9980	2.78	165
80502	0.7301	0.4243	1.0-1.2	1.0-2.5	40.2	1.089	126.0	150.9	81.4	0.9971	7.69	200.2
80677	1.6435	0.3596	1.0-1.2	1.0-1.1	27.5	1.970	166.3	37.3	156.1	0.9788	3.55	233.1
80726	2.3322	0.6551	M	M	17.2	2.964	145.9	32.1	113.25	0.9992	2.86	223.7
80816	1.9934	1.0646	M	M	16.15	3.033	11.4	45.8	37.0	0.9998	2.85	206.4
81036	1.2415	0.8752	M	M	22.3	2.076	99.5	16.05	86.3	0.9886	3.40	221.4
81177	0.7378	2.0217	M	M	19.4	2.729	143.3	8.9	130.85	0.9987	3.93	235.8
81250	0.8789	1.8627	M	M	16.2	2.718	158.3	59.6	135.35	0.9877	2.93	190.2
81689	3.2507	1.6567	M	M	10.6	4.888	66.6	149	142.95	0.9997	2.85	244.0
81854	0.3082	0.9754	1.0-1.2	1.0-1.2	33.7	1.244	17.1	18.9	147.1	0.9846	6.17	174.0
82374	0.6088	0.7060	1.0-3.0	1.0-2.0	41.1	1.232	141.5	40.1	112.3	0.8289	6.25	259.0

Film#	P_+	P_-	$\left(\dfrac{dE}{dx}\right)_+$	$\left(\dfrac{dE}{dx}\right)_-$	θ	p	ϕ	η	χ	$\cos\alpha'$	W	Q
82425	1.3637	1.3271	M	M	17.8	2.658	96.3	157.8	103.55	0.9816	2.96	224.1
82569	0.6163	2.8823	M	M	16.9	3.477	19.9	20.8	14.75	0.9992	2.79	254.3
83091	0.8384	2.0296	M	M	18.9	2.836	142.6	87.3	45.75	0.9973	2.89	249.7
83200	0.3447	1.4371	1.0-1.5	1.0-1.5	28.0	1.749	125.5	38.7	163.3	0.9788	3.94	208.2
83802	1.3319	1.2642	M	M	19.3	2.560	48.0	141.25	169.55	0.9958	3.01	237.1
84278	0.9736	2.5096	M	M	15.6	3.458	72.0	49.9	117.35	0.9922	3.78	243.5
84946	0.8570	1.6253	M	M	21.5	2.449	9.8	151.9	175.55	0.9899	3.07	219.3
84951	-.7398	0.5575	1.0-1.5	1.0-1.3	32.0	1.248	111.5	88.8	158.75	0.9543	6.06	173.4

The column grouping θ, p, ϕ, η, χ is headed by θ^0.

$$\theta^0$$

Neutron Production

Film #	p_+	p_-	$\left(\dfrac{dE}{dx}\right)_+$	$\left(\dfrac{dE}{dx}\right)_-$	θ	p	ϕ	η	χ	$\cos \alpha'$	W	Q
71939	1.9588	0.9124	M	M	16.8	2.842	129.1	18.9	147.1	0.9926	2.90	228.8
72240	0.0882	0.8077	3.5-5.0	1.0-1.1	56.3	0.850	114.8	55.1	180	0.9480	-	217.7
72487	0.7182	0.2319	1.0-1.1	1.0-1.1	51.2	0.882	167.8	157.4	11.2	0.9286	-	196.7
73016	1.6772	0.1848	1.0-1.1	1.0-1.2	16.5	1.856	128.3	74.75	145.5	0.9699	3.73	192.0
73593	0.3301	0.6675	1.0-1.1	1.0-1.1	35.5	0.958	153.1	54.5	173.6	0.9801	-	125.9
75560	0.5229	1.0134	1.0-1.3	1.0-1.3	36.4	1.471	81.9	97.8	15.6	0.9927	4.81	252.9
76257	0.2408	0.5507	1.1-1.3	1.0-1.1	76.6	0.650	21.4	154.4	115.0	0.8806	-	262.7
76321	1.0276	1.1524	M	M	19.4	2.148	62.7	150.9	147.15	0.9795	3.31	187.2
76573	0.1629	0.6265	1.0-1.1	1.0-1.1	59.9	0.722	22.1	144.3	121.3	0.9663	-	181.6
78398	0.4857	0.3820	1.0-1.1	1.0-1.1	41.3	0.812	148.1	161.6	40.8	0.8913	-	135.1
78778	0.7170	0.5720	1.0-1.1	1.0-1.3	38.4	1.217	64.8	124.9	170.05	0.9887	6.29	229.7
79351	1.3592	0.3944	1.0-1.5	1.0-1.5	28.9	1.715	168.7	156.3	12.6	0.9970	4.02	214.0
79436	0.6264	0.3674	1.0-1.1	1.0-1.1	52.3	0.900	157.7	173.7	28.55	0.9968	-	232.2
79519	0.8215	0.5032	1.0-1.1	1.0-1.1	38.0	1.257	149.9	124.8	38.4	0.9475	6.06	229.1

$$\theta^0$$

Proton Production

Film #	p_+	p_-	$\left(\dfrac{dE}{dx}\right)_+$	$\left(\dfrac{dE}{dx}\right)_-$	θ	p	ϕ	η	χ	$\cos \alpha'$	W	Q
88221	0.5195	0.8094	1.0-1.2	1.0-1.2	45.1	0.878	155.1	59.05	35.1	0.9440		294.2

Table IX. Anomalies

Film	p_+	p_-	θ	p	$\left(\dfrac{dE}{dx}\right)_+$	$\left(\dfrac{dE}{dx}\right)_-$	$Q(\pi\pi)$	$Q(e^+e^-)$	$Q(P^+e^-)$	$Q(n^+e^-)$
73456	0.5360	0.2626	36.4	0.7634	1.0-1.2	1.0-1.1	96.0±8.5	468±.5	-	-
75736	1.6315	0.0836	67.3	1.6655	1.0-1.5	1.0-1.5	-	-	100±19	300±56
79497	0.3020	1.3549	15.8	1.6475	1.0-1.1	1.0-1.1	118 ±16.2	173±18	-	-
81896	0.1408	0.2975	64.4	0.4171	1.1-1.5	1.0-1.1	101.9± 7.6	-	-	-

C. Error due to Nonuniformity of Magnetic Field

From a well-known formula of analytic geometry, the radius of curvature R of a curve $y = y(x)$ is related to the derivatives of y along the curve by

$$\frac{1}{R} = \frac{\frac{d^2 y}{dx^2}}{\left(1 + (\frac{dy}{dx})^2\right)^{3/2}} \cdot \qquad \text{(C-1)}$$

We are interested in the representation in analytic form of a cloud-chamber track, and can put the x axis along the chord joining the ends of the track:
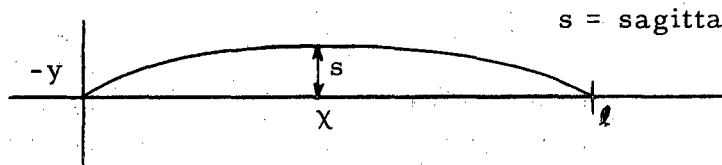
For a curve of large R, or more precisely for $s \ll 1$, the slope $\frac{dy}{dx}$ is small, and if we neglect it in comparison with 1, Eq. (C-1) becomes

$$\frac{1}{R} \cong \frac{d^2 y}{dx^2} \qquad \text{(C-2)}$$

in a magnetic field, $p = BR$, where p is the momentum, R is the instantaneous radius of curvature, and B is the magnetic field multiplied by certain constant factors.

Thus we have

$$\frac{d^2 y}{dx^2} = B/p. \qquad \text{(C-3)}$$

For a high-energy particle for which p is essentially constant, in a uniform magnetic field, Eq. (C-3) integrates to

$$y(x) = \frac{Bx^2}{2p} ; \qquad \text{(C-4)}$$

when $x = \ell/2$, then $y(\ell/2) = s$, the sagitta, and we have

$$p = \frac{B\ell^2}{8s} , \qquad \text{(C-5)}$$

the well-known approximate formula. Thus the considerations of this section, which will use Eq. (C-2), have the same range of validity as this customary high-energy approximation.

We wish to investigate the influence of nonuniformities in B on the values of p obtained by Eq. (C-5), and to determine, if possible, a suitable choice of B in the presence of nonuniformities, to insert in Eq. (C-5) in order to minimize the error involved in its use.

(I) A Linear Variation in B

$$B(x) = B_0 + ax;$$

inserting this in Eq. (C-3), we have

$$py''(x) = B_0 + ax ,$$

$$py(x) = \frac{B_0 x^2}{2} + \frac{ax^3}{6} + bx , \quad \text{for the curve of Fig. 1.}$$

The constant b can be evaluated from the requirement that $y(\ell) = 0$ in the coordinate system being used. This gives

$$b = \frac{-\ell}{2} \left(B_0 + \frac{a\ell}{3} \right) ,$$

and the formula for the sagitta (absolute value) becomes

$$ps = \frac{B_0 \ell^2}{8} + \frac{a\ell^3}{16} . \tag{C-6}$$

The customary formula $ps = \frac{B\ell^2}{8}$ gives the same value of p as Eq. (C-6) if B is chosen so that we have

$$\frac{B_0 \ell^2}{8} + \frac{a\ell^3}{16} - \frac{B\ell^2}{8} = 0$$

or

$$B = B_0 + a\ell/2 .$$

This is the field value at the center of the track.

(II) A Quadratic Variation in B

We have

$$B = B_0 + a(x - x_1)^2 .$$

Again, inserting in Eq. (C-3), we obtain

$$py''(x) = B_0 + a(x - x_1)^2 = B_0 + ax^2 - 2ax\,x_1 + ax_1^2 ,$$

and, integrating, we get

$$py(x) = (B_0 + ax_1^2)\frac{x^2}{2} = 2ax_1\frac{x^3}{6} + \frac{ax^4}{12} + bx . \qquad (C-7)$$

Again setting $y(\ell) = 0$ yields

$$B = \ell\left(ax_1\frac{\ell}{3} - \frac{a\ell^2}{12} - \frac{B_0 + ax_1^2}{2}\right) .$$

If one assumes that the quadratic field variation is about the center of the track, then we have $x_1 = \frac{\ell}{2}$, $B_0 = B_m$, the field at the center of the track, and

$$-b = \frac{\ell}{2}\left(B_m + \frac{a\ell^2}{12}\right) .$$

Inserting this in Eq. (C-7) and setting $x = \frac{\ell}{2}$ to obtain the quadratic sagitta formula, we find that Eq. (C-7) reduces to

$$ps = \frac{B_m\ell^2}{8} + \frac{a\ell^4}{192} .$$

The error in using the formula $ps = \frac{B_m\ell^2}{8}$ is

$$\Delta p = \frac{a\ell^2}{192} , \qquad\qquad (C-8)$$

$$\frac{\Delta p}{p} = \frac{a\ell^2}{24B_m} = \frac{1}{6}\left(\frac{a\ell^2}{4B_m}\right) .$$

Since the term in parentheses is the maximum quadratic field variation, Eq. (C-8) yields the result that the percentage error in p arising from use of the value of the field at the center of the track in the presence of a quadratic variation in the field is one-sixth the maximum percentage variation in B.

The variations in the 36-atmosphere chamber magnetic field are smooth, and can be well represented along a track by a sum of linear and quadratic terms. Consequently the foregoing analysis should provide a useful maximum error estimate.

D. Effect of Nucleon Motion in the Nucleus
·on the Distribution of Angles
Between Production and Decay Planes

At the energies of production considered here the effect of the "Fermi momentum" of the nucleons in the nucleus would not be expected to completely obliterate polarization effects as it would at lower energies, but the effect might be substantial, nonetheless. Hence it is interesting again to obtain an order-of-magnitude idea of the effect that nucleon motion might have on the angular distribution of particles scattered from, or produced in interaction with, such moving nucleons.

Consider the vector diagram:

Here $\vec{p}_i$ is the momentum of an incident particle such as a pion, $\vec{p}_n$ is the momentum of the nucleon in the struck nucleus, and $\vec{p}_r$ is the resultant momentum. We are concerned with the deviation of $\vec{p}_r$ from $\vec{p}_i$, represented by the angle θ. Assuming $\left|\vec{p}_i\right| \gg \left|p_n\right|$, we have

$$p_r \sin\theta \cong p_i \theta = p_n \sin\phi .$$

Averaging over ϕ, considering the p_n randomly distributed in ϕ, we obtain

$$(\overline{p_r \sin\theta})^2 = (\overline{p_n \sin\phi})^2 = \tfrac{1}{2}p_n^2 \cong p_i^2 \theta^2$$

or

$$\theta_{rms} = \sqrt{\overline{\theta^2}} = 1/2 \, p_n/p_i \cong 0.707 \times 0.216/4.5 = 0.0336 \cong 1.90$$

for an incident pion of 4.5 Bev/c momentum.

Now consider an angular distribution generated in a frame of reference that is displaced by the above amount from the one in which it is observed. That is, say, it is generated with respect to $(\vec{p}_r)_{av}$ and observed along $\vec{p}_i$, and then averaged for random distribution of $(\vec{p}_r)_{av}$ around $\vec{p}_i$ on a cone of half width θ_{rms}.

The following diagram illustrates the situation:
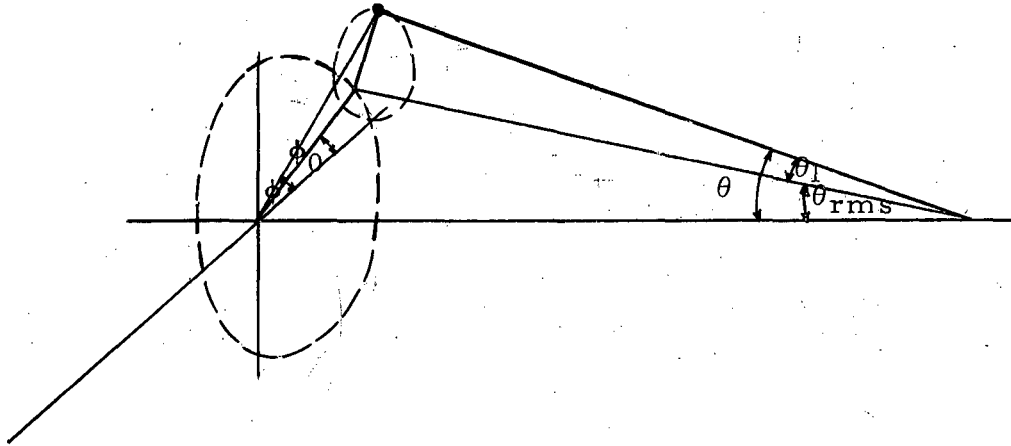
The angular distribution is observed as a function of θ, but generated as a function of θ_1. One can derive the following geometric relationship between the angles illustrated above:

$$\cos \theta_1 = \cos \theta_{rms} \cos \theta + \sin \theta \sin \theta_{rms} \cos (\phi - \phi_0). \quad (D-1)$$

If, then, it is desired to express an angular distribution in $\cos \theta_1$ in terms of $\cos \theta$, $\frac{d\sigma}{d\Omega} = f(\cos \theta_1)$, say, it can be done by replacing $\cos \theta_1$ by the expression (1) and then averaging over ϕ_0, holding ϕ fixed.

The distributions generated from simple cosine terms after averaging over ϕ are

$$\cos \theta_1 \rightarrow \cos \theta \cos \theta_0 ,$$

$$\cos^2 \theta_1 \rightarrow \cos^2 \theta \cos^2 \theta_0 + 1/2 \sin^2 \theta \sin^2 \theta_0 ,$$

$$\cos^3 \theta_1 \rightarrow \cos^3 \theta \cos^3 \theta_0 + 3/2 \sin^2 \theta \sin^2 \theta_0 ,$$

$$\cos^4 \theta_1 \rightarrow \cos^4 \theta \cos^4 \theta_0 + 3/2 \sin^2 \theta \sin^2 \theta_0 + 3/8 \sin^4 \theta \sin^4 \theta_0 .$$

For $\theta_{rms} = 1.9°$, the effect is small, but it increases rapidly as θ_{rms} increases.

E. Effect of Double Collisions in the Parent Nucleus

The information that can be derived from V^0's produced in heavy nuclei is complicated by the possibility of interactions in the nucleus other than the production interaction. The incident particle responsible for the production might, for instance, scatter from one nucleon before interacting with another to produce the V^0. The V^0, after having been made, might also scatter from a nucleon before emerging from the nucleus. To obtain an idea of the order of magnitude of such effects, it is interesting to consider the V^0 as having been made by a pion that first elastically scatters from another nucleon in the nucleus. After the pion has had one collision in the nucleus, it cannot afterward interact with any of the remaining nucleons behind it since it has already passed these. Assuming that on the average it can interact with half the nucleons in the nucleus after making the first collision, the fraction of second collisions to be expected per collision is

$$f \cong \frac{A}{2\pi r_0^2 A^{2/3}} \sigma_{(elastic)}^{(\pi - p)} = \frac{A^{1/3} \sigma_{el.}}{2\pi r_0^2} .$$

For copper, taking $\sigma_{el.} = 4 \times 10^{-27} cm^2$, [17] we obtain

$$f \cong \frac{(65)^{1/3} \times 4 \times 10^{-27}}{2\pi \times (1.4 \times 10^{-13})^2} \cong 13\% .$$

From the angular distribution of elastic scattering at this energy, [1]

$$\frac{d\sigma}{d\Omega} \cong \left| \frac{2J_1 (k a \sin \theta)}{k a \sin \phi} \right|^2 ,$$

where $a = 8 \times 10^{-14}$ cm, one can astertain that the median scattering angle is about 5°; that is, half the scatters are less than, half greater than, about 5°. One might take this median angle as an order-of-magnitude estimate of the angular error to be expected from such a double scattering process.

Both of these numbers, f and the median angular error, are less than the usual experimental uncertainties in making measurements of the type concerned here, but not enough less to be definitely negligible.

F. Effect of Precession on the Distribution of Angles
Between Production and Decay Planes

If, owing to a magnetic moment, the plane of decay of, say, a V^0 should precess about the magnetic field in a cloud chamber, then the distribution-in-angle of the angle between the plane of decay and the plane of production would be affected. It thus becomes necessary to study what this effect might be before attempting to interpret such an angular distribution.
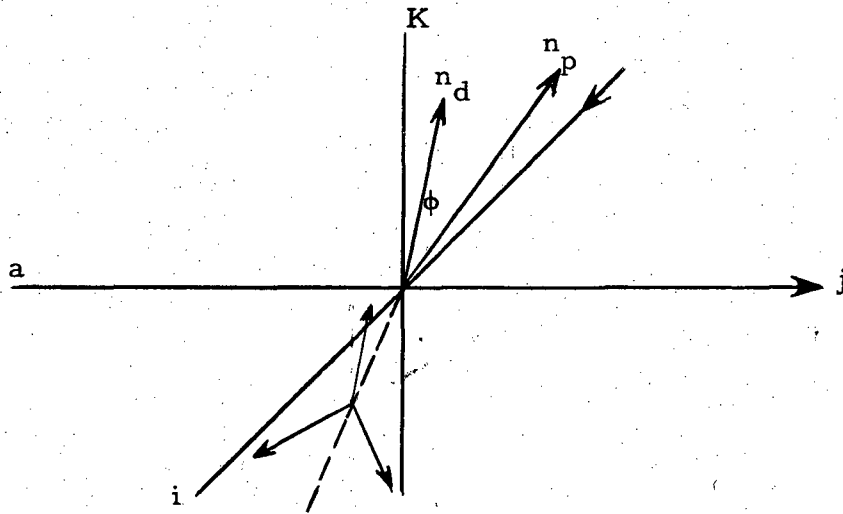
Let the i axis be the direction of a particle producing a V^0 at the origin. Let $\vec{n}_p$ be the unit normal to the production plane, $\vec{n}_d$ be the normal to the decay plane; ϕ is the angle between these two planes. Let us assume that the normals n_d are randomly distributed about n_p in azimuthal angle, so they form a cone of half angle ϕ.* Let us further assume that the normals n_d precess about $\vec{K}$. The effect of this precession on ϕ, then, would be that ϕ would increase, decrease, or remain the same depending on the position of n_d around the cone, the amount of precession, and the position of n_p relative to $\vec{K}$. For small angles of precession, because of the random distribution of n_d about n_p, one might expect the effect on ϕ to be a spreading of the values of ϕ uniformly from $\phi - \theta$ to $\phi + \theta$, where θ is the angle of precession.

---

*These normals belong to the different angles of emission of the V^0 that lie in the same production plane.

Thus if the original distribution in ϕ is $n(\phi)$, then the height of the curve n at the point ϕ due to those angles that are unchanged by precession becomes $n' = \frac{n(\phi)}{2\theta}$; to this must be added a contribution from those values $n'(\phi + \delta\phi)$ for $-\theta \leq \delta\phi \leq +\theta$, since some of all these angles will have the value ϕ after applying the precession. Thus, if we call the new distribution $N(\phi)$, we get

$$N(\phi) = \frac{1}{2\theta} \int_{\phi-\theta}^{\phi+\theta} n(\phi') \, d\phi' \ .$$

Obviously as $\theta \to 0$, $N \to n$. This can be interpreted as a simple averaging or "smearing" effect. Applying this to a simple distribution of the form $a + b \cos^2 \phi$, one obtains

$$N(n) = \frac{1}{2\theta} \int_{\phi-\theta}^{\phi+\theta} (a + b \cos^2 \phi') \, d\phi' = a + \frac{b}{2\theta}\left[\theta + \frac{1}{2} \sin 2\theta \cos 2\phi\right]$$

$$= a + \frac{b}{2}\left[1 + (\frac{\sin 2\theta}{2\theta}) \cos 2\phi\right] \ .$$

Thus as long as 2θ is in the "small angle" approximation region where $\frac{\sin 2\theta}{2\theta} \cong 1$ the distribution remains unchanged, since $\frac{1 + \cos 2\phi}{2} = \cos^2 \phi$. For $\theta \sim 10^\circ$, as discussed by Goldhaber,[33] $\frac{\sin 2\theta}{2\theta} \cong 0.98$.

For $\theta \sim 45^\circ$: $\frac{\sin 2\theta}{2\theta} \cong 0.90$.

Therefore this effect would appear negligible unless θ should be unusually large. It would reduce the height of a peak in a non-isotropic distribution, but would not affect a flat distribution.

BIBLIOGRAPHY

1. G. D. Rochester and C. C. Butler, Nature 160, 855 (1947).

2. R. W. Thompson, Proceedings of July 1955 Pisa Conference, to be published in Nuovo Cimento.

3. M. Ruderman and R. Karplus, Phys. Rev. 102, 247 (1956).

4. Fowler, Shutt, Thorndike, and Whittemore, Phys. Rev. 98, 121 (1955).

5. Walker, Preston, Fowler, and Kraybill, Phys. Rev. 97, 1086 (1955).

6. W. D. Walker and W. D. Shepard, Phys. Rev. 101, 1810 (1956).

7. Elliot, Maenchen, Moulthrop, Oswald, Powell, and Wright, Rev. Sci. Instr. 26, 696 (1955).

8. Proceedings of the Sixth Annual Rochester Conference on High-Energy Nuclear Physics (to be published).

9. Proceedings of the Fifth Annual Rochester Conference on High-Energy Nuclear Physics, Interscience, New York, 1955.

10. Proceedings of the 1954 Glasgow Conference, Pergamon Press, London.

11. M. Gell-Mann and A. Pais, Phys. Rev. 97, 1387 (1955).

12. Osher, Moyer, and Parker, Bull. Am. Phys. Soc. 1, 185 (1956).

13. Leighton, Wanlass, and Anderson, Phys. Rev. 89, 148 (1955).

14. Fretter, May, and Nakada, Phys. Rev. 89, 168 (1953).

15. C. C. Butler, Progress in Cosmic Ray Physics, (1952) Chapter II, North Holland Publishing Co., Amsterdam.

16. Fowler, Maenchen, Powell, Saphir, and Wright, Phys, Rev. 101, 911 (1956).

17. Maenchen, Powell, Saphir, and Wright, Phys. Rev. 99, 1619 (1955).

18. W. B. Fowler, G. Maenchen, W. Powell, G. Saphir, and R. W. Wright, Production of a θ^0 Particle without an Associated Hyperon in a π^--p Collision, UCRL-3321, Feb. 1956.

19. Wright, Saphir, Powell, Maenchen, and Fowler, Bull. Am. Phys. Soc. 30, 18 (1955).

20. P. H. Moulthrop, Pion Production by Neutrons on Helium (Thesis), UCRL-2858, Jan. 1955.

21. Breuckner, Hartsough, Hayward, and Powell, Phys. Rev. 75, 555 (1949).

22. M. O. Fuller, Disintegration of Oxygen by 300-Mev Neutrons, (Thesis), UCRL-2699, Sept. 1954.

23. Ballam, Grisaru, and Treiman, Phys. Rev. 101, 1438 (1956).

24. Block, Harth, and Blevins, Phys. Rev. 100, 959 (1955).

25. Slaughter, Harth, and Block, Bull. Am. Phys. Soc. I, 64 (1956).

26. G. H. Trilling and R. B. Leighton, Phys. Rev. 100, 1468 (1955).

27. S. B. Treiman and H. W. Wyld, Jr., Phys. Rev. 100, 879 (1955).

    (a) Treiman, Reynolds, and Hodson, Phys. Rev. 97, 244 (1955).

28. M. S. Bartlett, Phil. Mag. 44, 249 (1953).

29. D. B. Gayther and C. C. Butler, Phil. Mag. 46, 467 (1955).

30. Gupta, Snyder, and Chang, Bull. Am. Phys. Soc. 1, 186 (1956).

31. Prof. Malvin A. Ruderman, private communication.

32. Deutschmann, Cresti, Greening, Guerriero, Loria, and Zago, Nuovo Cimento III, 566 (1956).

33. M. Goldhaber, Phys. Rev. 101, 1828 (1956).

34. R. Jastrow, Phys. Rev. 97, 181 (1955).

35. H. Blumenfeld, E. T. Booth, L. M. Lederman, and W. Chinowsky, Preprint in advance of publication.

36. G. Maenchen and R. W. Wright, private communication.

37. I am indebted to George Maenchen for suggesting these ideas.